Phase state and viscosity of secondary organic aerosols over China simulated by WRF-Chem

Zhiqiang Zhang[1,2], Ying Li[1], Haiyan Ran[1,2], Junling An[1], Yu Qu[1], Wei Zhou[1], Weiqi Xu[1], Weiwei Hu[3], Hongbin Xie[4], Zifa Wang[1], Yele Sun[1], Manabu Shiraiwa[5]

[1]State Key Laboratory of Atmospheric Boundary Layer Physics and Atmospheric Chemistry, Institute of Atmospheric Physics, Chinese Academy of Sciences, Beijing 100029, China

[2]College of Earth and Planetary Sciences, University of Chinese Academy of Sciences, Beijing 100049, China

[3]State Key Laboratory of Organic Geochemistry, Guangzhou Institute of Geochemistry, Chinese Academy of Sciences, Guangzhou 510640, China

[4]Key Laboratory of Industrial Ecology and Environmental Engineering (Ministry of Education), School of Environmental Science and Technology, Dalian University of Technology, Dalian 116024, China

[5]Department of Chemistry, University of California, Irvine, CA 92697-2025, USA

Correspondence to: Ying Li (liying-iap@mail.iap.ac.cn)

Abstract. Secondary organic aerosols (SOA) can exist in liquid, semi-solid or amorphous solid states, which are rarely accounted for in current chemical transport models (CTMs). Missing the information of SOA phase state and viscosity in CTMs impedes accurate representation of SOA formation and evolution, affecting the predictions of aerosol effects on air quality and climate. We have previously developed a parameterization to estimate the glass transition temperature (T_g) of an organic compound based on volatility and to predict viscosity of SOA. In this study, we apply this method to predict the phase state of SOA particles over China in summer of 2018 using the Weather Research and Forecasting model coupled to Chemistry (WRF-Chem). This is the first time that spatial distributions of the SOA phase state over China are investigated by a regional CTM. Simulations show that T_g values of dry SOA range from ~287 K to 305 K, with higher values in the northwestern China where SOA particles have larger mass fractions of low volatility compounds. Considering water uptake by SOA particles, the SOA viscosity shows a prominent geospatial gradient that highly viscous or solid SOA particles are mainly predicted in the northwestern China. The lowest and highest SOA viscosity values both occur over the Qinghai-Tibet Plateau that the solid phase state is predicted over dry and high-altitude areas and the liquid phase state is predicted mainly in the south of the plateau with high relative humidity during the summer monsoon season. We also calculate the characteristic mixing timescale of organic molecules in 200 nm SOA particles to evaluate kinetic limitations in SOA partitioning. Calculations show that during the simulated period the percent time of the mixing timescale longer than 1 h is > 70 % at the surface and at 500 hPa in most areas of the northern China, indicating that kinetic partitioning considering the bulk diffusion in viscous particles may be required for more accurate prediction of SOA mass concentrations and size distributions over these areas. Sensitivity simulations show that including the formation of extremely low-volatile organic compounds, the percent time that a SOA particle is in the liquid phase state decreases by up to 12 % in the southeastern China during the

33 simulated period. With an assumption that the organic and inorganic compounds are internally mixed in one phase, we show

34 that the water absorbed by inorganic species can significantly lower the simulated viscosity over the southeastern China.

35 This indicates that constraining the uncertainties in simulated SOA volatility distributions and the mixing state of the organic

36 and inorganic compounds would improve prediction of viscosity in multicomponent particles in southeastern China.

37 **1 Introduction**

38 Secondary organic aerosols (SOA) are major components of atmospheric fine particles, impacting air quality, climate and

39 public health (Jimenez et al., 2009; Pöschl and Shiraiwa, 2015). The formation and evolution of SOA involve both chemical

40 reactions and mass transport in the gas and particle phases (Ziemann and Atkinson, 2012). This complexity makes accurate

41 representation of SOA evolution in chemical transport models (CTMs) challenging, leading to a large uncertainty in

42 evaluating SOA impacts on air quality and climate (Kanakidou et al., 2005; Shrivastava et al., 2017).

43 Current CTMs usually assume that SOA particles are homogeneous and well-mixed liquids, with rapid establishment of

44 gas–particle equilibrium applied in simulations of SOA formation and partitioning (Pankow, 1994; Donahue et al., 2006). It

45 has been shown that SOA can exist in liquid (low dynamic viscosity η, $\eta < 10^2$ Pa s), semi-solid (10^2 Pa s $\leq \eta \leq 10^{12}$ Pa s) or

46 solid (amorphous or glassy solid; $\eta > 10^{12}$ Pa s) states, depending on particle chemical composition and atmospheric

47 conditions, such as ambient temperature (T) and relative humidity (RH) (Koop et al., 2011; Reid et al., 2018). Viscosities can

48 be converted to bulk diffusion coefficients via the Stokes-Einstein equation (Einstein, 1905; Seinfeld and Pandis, 2016) or

49 the fractional Stokes-Einstein equation (Price et al., 2016; Evoy et al., 2019; Evoy et al., 2020). The phase state, viscosity,

50 and bulk diffusivity of SOA are important in many aerosol processes. The semi-solid or solid phase state can prolong the

51 equilibration timescales in the gas-particle partitioning, indicating a need of considering kinetic limitations in simulating the

52 SOA partitioning into highly viscous particles (Shiraiwa and Seinfeld, 2012; Roldin et al., 2014; Zaveri et al., 2014; Li and

53 Shiraiwa, 2019). The viscosity of SOA can impact the rates of heterogeneous and multiphase reactions (Marshall et al., 2018;

54 Zhang et al., 2019a), photochemistry (Liu et al., 2018; Dalton and Nizkorodov, 2021; Baboomian et al., 2022), and the

55 uptake of gaseous pollutants (e.g., O_3, OH, N_2O_5, NO_2, NH_3, and SO_2) and water vapor (Abbatt et al., 2012; Kuwata and

56 Martin, 2012; Preston and Zuend, 2022), with implications for accurate predictions of atmospheric chemical composition

57 (Reid et al., 2018). The SOA phase state also affects particle size distribution evolution (Shiraiwa et al., 2013; Zaveri et al.,

58 2022) and ice nucleation pathways (Knopf and Alpert, 2023).

59 Accurate predictions of the viscosity need the information of molecular structures and functional groups (Song et al.,

60 2016; Rothfuss and Petters, 2017; Gervasi et al., 2020; Galeazzo and Shiraiwa, 2022); however, molecular specificity is

61 often unavailable in ambient measurements, leading to the prediction of the phase state of ambient SOA particles difficult.

62 Currently there are only a few methods developed to predict the phase state of ambient SOA particles, and successfully be

implemented in CTMs. Li, Shiraiwa and coauthors first developed a parameterization predicting the glass transition temperature (T_g) based on the molar mass (M) and the atomic O/C ratio for carbon-hydrogen (CH) and carbon-hydrogen-oxygen (CHO) compounds with their molar mass less than 450 g mol^{-1} (Shiraiwa et al., 2017). T_g characterizes the temperature at which a phase transition between amorphous solid and semi-solid states occurs (Koop et al., 2011). When the ambient T is higher than T_g, a SOA particle is in a semi-solid or liquid phase state; otherwise, it behaves as an amorphous solid. This parameterization has been successfully coupled into CTMs simulating the SOA phase state over the globe (Shiraiwa et al., 2017) or the U.S. (Schmedding et al., 2020; Li et al., 2021b), showing that semi-solid and amorphous solid phase states frequently occurred over dry lands and in the upper troposphere. Further parameterizations were developed to predict T_g as a function of the saturation mass concentration (C^0) and the O/C ratio of organic compounds, or as a function of C^0 solely, which indirectly included the effect of molecular structure on T_g estimations (Li et al., 2020). This parameterization can be used in the volatility basis set (VBS) framework (Donahue et al., 2006), which is widely adopted in CMTs simulating SOA formation (Lane et al., 2008a; Knote et al., 2015). Rasool et al. (2021) then coupled this new method (Li et al., 2020) into the Weather Research and Forecasting Model coupled to chemistry (WRF-Chem) (Grell et al., 2005; Fast et al., 2006), and the simulations showed that the viscosity of SOA particles could be reasonably predicted during the dry-to-wet transition season in the Amazon rainforest. Li et al. (2020) was also applied in the WRF-Chem simulating the effects of particle phase state on the multiphase chemistry of SOA formation in the Amazon rainforest (Shrivastava et al., 2022; Rasool et al., 2023). Instead of predicting T_g, Maclean et al. (2021) developed parameterizations for viscosity as a function of T and RH based on measured viscosity data of laboratory SOA, and applied the viscosity parameterizations in CTMs to predict the mixing timescales of organic molecules and water molecules within SOA particles on a global scale (Maclean et al., 2017; Maclean et al., 2021). It is needed to conduct more simulations to investigate the SOA phase state varied with locations and the time. Simulations of the SOA phase state in China on a regional scale have not been available.

Investigations in the particle phase state over China are currently focused on field observations and laboratory experiments. Bounce factor measurements showed that submicrometer particles can be semi-solid in clear days and liquid in hazy days in Beijing, China (Liu et al., 2017). The phase state of PM$_{2.5}$ (particulate matter with an aerodynamic diameter $\leq$ 2.5 μm) was found to be mostly semisolid to solid in winter Beijing based on the measurements using optical microscopy combined with the poke-and-flow technique (Song et al., 2022). The RH-dependent viscosity of the proxies of actual ambient particles in Beijing was also investigated based on dual optical tweezers (Tong et al., 2022). The phase state of submicrometer particles in Beijing was retrieved from a polarization lidar that has the potential to infer the vertical profiles of phase state (Tan et al., 2020). The phase state of traffic-related secondary aerosols in Beijing may have a distinguished diurnal variation (Meng et al., 2021). The biomass burning aerosols, collected near a farmland in Yangtze River Delta, China, were found to exist in the non-solid phase state at relatively dry conditions (Liu et al., 2021).

95 These measurements indicate that the particle phase state over China is highly variable under different atmospheric

96 conditions. It is important to know the spatial distributions and time variations of the SOA phase state and viscosity in

97 multicomponent particles to better quantify the aerosol effects on air quality, which, however, has not been investigated over

98 China with air quality models on a regional scale. Here we use the WRF-Chem model simulated SOA volatility distributions

99 to estimate the glass transition temperature and viscosity of SOA particles over China based on the parameterizations

100 developed in Li et al. (2020). We further calculate the diffusion coefficients and mixing timescales of organic molecules

101 within SOA, which has implications in how to properly treat the SOA partitioning (instantaneous equilibrium vs. kinetic

102 partitioning) in CTMs. As volatility and viscosity are closely related, we conduct a sensitivity calculation to evaluate the

103 effects of the simulated SOA volatility distributions on viscosity estimations. We also conduct a sensitivity calculation to

104 investigate how the water absorbed by inorganic components in $PM_{2.5}$ affects viscosity estimations, which has implications

105 in predicting the viscosity of internally mixed ambient particles.

106 **2 Methods**

107 **2.1 WRF-Chem model configuration**

108 We use the WRF-Chem model version 3.7.1 (Grell et al., 2005; Fast et al., 2006) and simulate the period from 20 May to 23

109 June 2018 with a spin-up period of 7 days (May 13 – 19). We set up two domains (Fig. S1 in the Supplement) with the

110 horizontal resolutions of 81 km and 27 km, respectively, and 18 vertical layers are applied from the surface up to 100 hPa.

111 The meteorological initial and boundary conditions are from the National Centers for Environmental Prediction (NCEP)

112 Global Forecast System (GFS) final (FNL) reanalysis data. The outputs of a global chemical transport model MOZART-4

113 (Emmons et al., 2010) provide initial and boundary conditions of chemical species over the outer domain (Fig. S1 in the

114 Supplement). Anthropogenic emissions are from the MIX 2010 inventory for Asia (Li et al., 2017) and the MEIC 2016

115 inventory for China (http://meicmodel.org.cn) (Zheng et al., 2018). Biogenic emissions are calculated from the Model of

116 Emissions of Gases and Aerosols from Nature (MEGAN2.1) (Guenther et al., 2012).

117 The utilized physical and chemical schemes are given in Table S1. We use the MOZART-4 mechanism (Emmons et al.,

118 2010) for the gas-phase chemistry. The MOSAIC (Model for Simulating Aerosol Interactions and Chemistry) aerosol module

119 (Zaveri et al., 2008) is applied for the aerosol chemistry and we represent aerosol particles with 4-size sections having dry

120 diameters ranging from 0.039 μm to 10 μm (Knote et al., 2015). SOA formation is treated with the 1-D volatility basis set

121 (VBS) approach (Donahue et al., 2006) which has been implemented into the MOSAIC aerosol module (Lane et al., 2008a;

122 Ahmadov et al., 2012). Five volatility bins are considered (effective saturation mass concentrations C^* of 10^{-4}, 1, 10, 100,

123 and 1000 μg m^{-3} at 298 K) in the official version 3.7.1 of the WRF-Chem model, with the enthalpy of vaporization (ΔH_{vap})

124 values of 40, 131, 120, 109, and 98 kJ mol^{-1} used in each volatility bin (Knote et al., 2015). We follow Knote et al. (2015)

125 with SOA mass yields adopted for four volatility bins (1, 10, 100, and 1000 μg m^{-3}). Further gas-phase aging is simulated

126 through OH oxidation of SOA vapors with a fixed rate of 1.0×10^{-11} cm^3 molec^{-1} s^{-1}, with products shifted down one

127 volatility bin (Murphy and Pandis, 2009), e.g., the condensable vapors with C^* of 1 μg m^{-3} react with OH forming surrogate

128 species in the lowest volatility bin (C^* of 10^{-4} μg m^{-3}). The partitioning of organic compounds between the gas and particle

129 phases is simulated based on Pankow (1994) which is implemented in MOSAIC (Shrivastava et al., 2011). We apply glass

130 transition temperature and viscosity calculations to WRF-Chem model output for traditional SOA formed from the oxidation

131 of volatile organic compounds including alkanes, alkenes, aromatics, isoprene, and monoterpenes (Lane et al., 2008b).

2.2 Glass transition temperature and viscosity calculations

133 The glass-transition temperature of SOA products in each volatility bin at dry conditions ($T_{g,i}$) is calculated as a function of

134 the saturation mass concentration at 298 K (C^0) using the parameterization (Eq. 1) developed in our previous study (Li et al.,

135 2020). We assume ideal thermodynamic mixing that C^0 is equal to C^*, which is often applied in the VBS (Donahue et al.,

136 2011).

$$T_{g,i} = 288.70 - 15.33 \times log_{10}(C^0) - 0.33 \times [log_{10}(C^0)]^2 \qquad (1)$$

137 The T_g of mixtures of dry SOA compounds ($T_{g,org}$) is calculated by the Gordon−Taylor equation (Gordon and Taylor,

138 1952), with the Gordon−Taylor constant (k_{GT}) assumed to be 1 (Dette et al., 2014):

$$T_{g,org} = \sum_i \omega_i T_{g,i} \qquad (2)$$

139 where ω_i is the mass fraction of SOA products in each volatility bin simulated by the VBS module in WRF-Chem.

140 The particle phase state depends strongly on water content in particles, as water can act as a plasticizer to decrease

141 viscosity (Mikhailov et al., 2009; Koop et al., 2011). The mass concentration of water absorbed by SOA particles under

142 humid conditions is estimated using the effective hygroscopicity parameter (κ) (Petters and Kreidenweis, 2007) as:

$$m_{H_2O} = \left(\frac{a_w}{1-a_w}\right)\frac{\kappa \rho_w m_{SOA}}{\rho_{SOA}} \qquad (3)$$

143 where a_w is water activity calculated as a_w = RH/100 and ρ_w is the density of water. m_{SOA} is the simulated total mass

144 concentrations of traditional SOA. The density of SOA particles (ρ_{SOA}) is assumed to be 1.5 g cm^{-3} (Knote et al., 2015). κ is

145 assumed to be 0.1 based on previous studies (Gunthe et al., 2009; Duplissy et al., 2011; Wu et al., 2013) and consistent with

146 the value used in our previous global SOA phase state simulations (Shiraiwa et al., 2017).

147 T_g of organic-water mixtures is also calculated by the Gordon−Taylor equation (Eq. 4) with k_{GT} suggested to be 2.5

148 (Koop et al., 2011).

$$T_g(\omega_{org}) = \frac{(1-\omega_{org})T_{g,w} + \frac{1}{k_{GT}}\omega_{org}T_{g,org}}{(1-\omega_{org}) + \frac{1}{k_{GT}}\omega_{org}} \qquad (4)$$

149 where ω_{org} is the mass fraction of the simulated SOA species in organic-water mixtures. The glass transition temperature of

150 pure water ($T_{g,w}$) is 136 K (Kohl et al., 2005). Based on $T_g(\omega_{org})$, viscosity can be calculated with the

151 Vogel−Tammann−Fulcher (VTF) equation (Angell, 1991): $\eta = \eta_\infty e^{\frac{T_0 D}{T - T_0}}$, where η_∞ is the viscosity at infinite temperature

152 (10^{-5} Pa s, Angell (1991)). D is the fragility parameter which is adopted to be 10 based on our previous study in DeRieux

153 and Li et al. (2018). T_0 is the Vogel temperature calculated as $T_0 = \frac{39.17 \; _g(\omega_{org})}{D + 39.17}$. We further calculate the bulk diffusion

154 coefficient (D_b) of organic molecules with a radius of 0.4 nm (Maclean et al., 2021) and water molecules in SOA particles

155 based on predicted viscosity and the fractional Stokes−Einstein equation (Price et al., 2016; Evoy et al., 2019; Evoy et al.,

156 2020), which is detailed in the Supplement. The mixing timescales of molecules (τ_{mix}) within SOA particles is calculated as

157 $\tau_{mix} = d_p^2/(4\pi^2 D_b)$ (Seinfeld and Pandis, 2016), where d_p is the particle diameter. The d_p is assumed to be 200 nm

158 (Maclean et al., 2021) when we calculate τ_{mix}.

159 **2.3 Sensitivity simulations**

160 Table 1 lists all the performed simulations. In the base case, we update the C^* in the lowest volatility bin from 10^{-4} µg m^{-3} in

161 the official WRF-Chem v3.7.1 to 0.1 µg m^{-3} based on the ambient volatility observations (referring to Section 2.4 and Fig. 1),

162 and calculate the ΔH_{vap} in the lowest volatility bin using the semi-empirical parameterization in Epstein et al. (2010), leading

163 to a value of 142 kJ mol^{-1}. To evaluate the effects of simulated SOA volatility distributions on phase state estimations, we

164 conduct a simulation (sensitivity case A) following the default setting in the model assuming that the lowest C^* is 10^{-4} µg m^{-}

165 ^{3} at 298 K, with ΔH_{vap} of 40 kJ mol^{-1} (Knote et al., 2015). A smaller ΔH_{vap} indicates less dependence of volatility on

166 temperature variations. In the sensitivity case B, we increase the simulated RH by a factor of 10 % as we find that the

167 simulated RH values are smaller than the observations (Section 3.1). In the base case and sensitivity cases A and B, we

168 predict T_g for SOA-water mixtures accounting for the SOA-influenced water uptake solely, assuming that SOA particles are

169 externally mixed with inorganic compounds such as sulfate and nitrate. In the sensitivity case C, we assume that the organic

170 and inorganic compounds are internally mixed in one phase and include the water absorbed by inorganic compounds in

171 viscosity calculations. The water associated with inorganics is calculated by the MOSAIC module coupled in WRF-Chem.

172 **2.4 Observation**

173 The observation data measured at an urban site in the Institute of Atmospheric Physics (IAP), Chinese Academy of Sciences

174 (39°58′28″ N, 116°22′16″ E) in Beijing (Fig. S1 in the Supplement) are used to compare with the simulation results of the

175 WRF-Chem model. The aerosol volatility was measured from 20 May to 23 June in 2018, using a thermodenuder coupled

with an Aerodyne high-resolution aerosol mass spectrometer (Xu et al., 2019). The volatility distributions of oxygenated organic aerosols (OOA) resolved from positive matrix factorization (PMF) were estimated using a dynamic mass transfer model (Riipinen et al., 2010). The volatility of OOA was found to be distributed in six logarithmically spaced C^* bins including 0.001, 0.01, 0.1, 1, 10, and 100 μg m^{-3}, based on the best fits between the measured and predicted thermograms using the methods in Karnezi et al. (2014). Chemical species including organics (Org), sulfate (SO$_4^{2-}$), nitrate (NO$_3^-$), and ammonium (NH$_4^+$) in PM$_{2.5}$ were measured using an Aerodyne time-of-flight aerosol chemical speciation monitor (Fröhlich et al., 2013) equipped with a capture vaporizer and PM$_{2.5}$ lens, with the details described in Li et al. (2023). The OOA factor was identified with the PMF analysis. We obtain the mass concentrations of PM$_{2.5}$ from the Olympic Center observation site (http://zx.bjmemc.com.cn) which is ~4 km from the IAP site (Fig. S1 in the Supplement). Meteorological parameters including RH and T are from the Beijing meteorological tower at the IAP site.

3 Results

3.1 Simulations in Beijing and the comparison with observations

The comprehensive model evaluations were conducted in our previous studies, showing that the WRF-Chem model reasonably captured the magnitudes and spatial distributions of concentrations of major air pollutants over China (Li et al., 2011; Li et al., 2014; Li et al., 2015; Qu et al., 2019; Zhang et al., 2022). Here we focus on the comparison of simulations and observations at the IAP site during 20 May – 23 June 2018 when the observed volatility distributions are available (Xu et al., 2019).

Figure 1 shows the average volatility distributions of observed OOA and simulated SOA at the IAP site. The C^* of OOA spans from 0.001 μg m^{-3} to 100 μg m^{-3}, with an average value of 1.16 μg m^{-3}. The semi-volatile organic compounds (SVOC; $0.3 < C^0 < 300$ μg m^{-3}) and the low-volatile organic compounds (LVOC; $3\times10^{-4} < C^0 < 0.3$ μg m^{-3}) (Donahue et al., 2012) contribute 66.3 % and 33.7 % to OOA concentrations, respectively (Xu et al., 2019). The $T_{g,org}$ estimated from the observed OOA volatility distributions is 286.7 K. Figure 1a shows the simulated volatility distributions of SOA with five C^* bins set to be 0.1, 1, 10, 100, and 1000 μg m^{-3} at 298 K, and ΔH_{vap} of 142, 131, 120, 109, and 98 kJ mol^{-1} used in the five C^* bins, respectively (base case in Table 1). In this base case simulation, the SOA consists of 64.5 % SVOC and 35.3 % LVOC, and most of the SVOC species are located in the C^* bin of 1 μg m^{-3}. The simulated SOA in Fig. 1a has an average C^* of 0.64 μg m^{-3} and $T_{g,org}$ of 291.5 K, close to the values estimated from the volatility distributions of OOA. Figure 1b shows the simulated volatility distributions of SOA with the lowest C^* bin set to be 0.0001 μg m^{-3} at 298 K with ΔH_{vap} of 40 kJ mol^{-1}, following the default option in the official WRF-Chem model 3.7.1 (Knote et al., 2015). In this sensitivity simulation (case A in Table 1), the SOA consists of 40.4 % extremely low-volatile organic compounds (ELVOC; $C^0 < 3\times10^{-4}$ μg m^{-3}), which are not determined in the observed OOA, leading to a much lower average C^* (0.03 μg m^{-3}) and a higher $T_{g,org}$ (309.0 K)

206 compared to the observations. In the following we estimate the $T_{g,org}$ and viscosity of SOA using the simulated volatility

207 distributions in the base case with the lowest C^* bin set as 0.1 µg m^{-3} at 298 K. The impacts of volatility distributions with

208 the incorporation of ELVOC (Fig. 1b) on viscosity estimations are evaluated in section 3.3.

209   Figure 2 shows that the model relatively well reproduces the observed hourly variations of RH, T, mass concentrations

210 of PM$_{2.5}$ and its major inorganic components (Figs. 2a – f), with the index of agreement (IOA, defined in the Supplement)

211 varied from ~0.70 for inorganic components to a higher value of 0.93 for T (Table S2 in the Supplement). The simulated

212 values of RH are constantly lower than the observations, with the mean bias (MB) being –10.97 % (Table S2 in the

213 Supplement). The underestimation of RH observations was also found at other meteorological sites in the North China Plain

214 in our previous studies (Qu et al., 2019; Zhang et al., 2022), which would affect the SOA viscosity estimations. The effects

215 of RH on the viscosity estimations are evaluated in section 3.3. Figure 2g shows that the model could generally reproduce

216 the observed temporal variations of OOA concentrations, but largely underestimates the observation peaks (MB = –5.88 µg

217 m^{-3}, the normalized mean bias NMB = –53.28 %, Table S2 in the Supplement). Incorporation of the SOA formed from

218 intermediate-volatile organic compounds (IVOCs) (Miao et al., 2021; Chang et al., 2022) would increase the simulated SOA

219 concentrations, which is beyond the scope of this study and will be considered in our future work. The simulated SOA mean

220 concentration is 5.15 µg m^{-3}. Although it is lower than the observed value of 11.03 µg m^{-3}, this difference in the simulated

221 and observed SOA concentrations would not affect the viscosity predictions significantly. The SOA viscosity has a much

222 closer relation with the volatility rather than its mass loadings (Champion et al., 2019; Li et al., 2020). In our previous study

223 we estimated $T_{g,org}$ and viscosities at different OA mass loadings varied from 1 to 1000 µg m^{-3}, showing that the simulated

224 viscosities were very similar, particularly when RH was higher than 50 % (DeRieux et al., 2018).

225   As the WRF-Chem model underestimates the observed RH at the IAP site, we calculate the SOA viscosity using the

226 simulated and observed RH, respectively. Figure 2h shows that the viscosities calculated at the two conditions are similar at

227 most times during the simulated period, ranging mainly from ~10^2 Pa s to 10^{10} Pa s, with a median value of ~10^7 Pa s,

228 indicating that a semi-solid phase state frequently occurs. The underestimations of the observed RH by WRF-Chem mainly

229 impact the phase state estimations at relatively high RH. For example, SOA particles occur as liquid when the observed RH

230 is higher than ~75 %; however, they remain in a semi-solid phase state at the simulated RH. The bulk diffusion coefficients

231 (D_b) of organic molecules range from 10^{-18} to 10^{-11} cm^2 s^{-1} at the simulated RH (Fig. 2i), leading to the mixing timescales

232 within 200 nm SOA particles being seconds to years, with 61 % of the time > 1 hour (Fig. S2 in the Supplement). We

233 highlight the mixing timescale of 1 hour as the time step adopted in CTMs is often ~ 0.5 – 1 hour (Maclean et al., 2021).

234 Current CTMs usually assume that the gas-particle partitioning of SVOCs reaches equilibrium quickly within the time step

235 (Pankow, 1994; Donahue et al., 2006). When the mixing timescales of organics within SOA particles are $\leqslant$ ~ 1 hour, the

236 instantaneous equilibrium is a reasonable assumption. However, when the mixing timescales of organics are longer than ~ 1

237 hour, non-equilibrium between the gas phase and the particle phase, i.e., the kinetic partitioning may need to be considered in

238 simulating the SOA formation in CTMs (Shiraiwa and Seinfeld, 2012; Zaveri et al., 2018; Li and Shiraiwa, 2019; Zaveri et

239 al., 2020; He et al., 2021; Jathar et al., 2021; Maclean et al., 2021; Shiraiwa and Pöschl, 2021; Shrivastava et al., 2022).

240   The vertical profiles of SOA viscosity exhibit diurnal variations. Figure 3a shows the median diurnal and vertical

241 profiles of predicted SOA viscosity at the IAP site. The SOA particles remain highly viscous ($\sim 10^7 - 10^8$ Pa s) at the surface,

242 with a higher viscosity occurring from late afternoon to early evening, during which the RH is less than 20 %, lower than the

243 rest time of the day (Fig. S3 in the Supplement). The SOA particles become more viscous at higher altitudes than the surface

244 and adopt the phase transition from a semi-solid phase to a solid phase at ~ 4 km at the IAP site. The predicted altitude with

245 the phase transition is ~ 2 km higher than our previous global model prediction for the region of East China which was an

246 average of five years' simulations (Shiraiwa et al., 2017). Tan et al. (2020) inferred the phase state of submicrometer

247 particles in Beijing from the surface to an altitude of ~ 1 km using a polarization lidar and found that the particle phase state

248 exhibits a vertical variation. Further observations of SOA viscosity at high altitudes are needed to better understand the

249 viscosity vertical profiles and validate our predictions. Figure 3b shows that the mixing timescales for organic molecules

250 within 200 nm SOA particles are approximately 1 hour at the surface, and longer than ~ 10 hours at altitudes higher than 1

251 km, indicating that kinetic limitations in the gas-particle partitioning may be required to accurately predict SOA mass

252 concentrations in summer Beijing, particularly in the upper planetary boundary layer and the free troposphere.

253 **3.2 Simulated glass transition temperature and viscosity of SOA particles over China**

254   The glass transition temperature of the dry organic phase ($T_{g,org}$) shows a geospatial gradient over China. Figure 4a shows the

255 median surface values of $T_{g,org}$ calculated in the base simulation (Table 1). $T_{g,org}$ ranges from $\sim 287 - 305$ K over most areas of

256 China, with lower values occurring mainly over the southeast and higher values over the northwest. The $T_{g,org}$ range

257 simulated by the WRF-Chem model is consistent with our previous global simulations of $T_{g,org}$ that varied from ~ 285 K to

258 310 K at the surface over China (Shiraiwa et al., 2017). The geospatial variation in $T_{g,org}$ is related to the simulated SOA

259 volatility distributions. Figure 4b shows the mass fractions of SOA species distributed in the lowest volatility bin (SOAX

260 with $C^* = 0.1$ µg m^{-3} at 298 K). The mass fractions of SOAX are mostly $20 - 35$ % in the southeastern China, indicating that

261 the majority of the simulated SOA formed from VOCs is semi-volatile. In these areas, the simulated SOA mass

262 concentrations are higher than the other locations of China (Fig. S4 in the Supplement) (Li et al., 2022), which is favorable

263 for more SVOCs partitioning into the particle phase, leading to relatively low values of $T_{g,org}$ (Fig. 4a). LVOCs are more

264 frequently contained in aged SOA particles in remote areas, e.g., some areas in the northwestern China where the SOA mass

265 concentrations are very low, resulted in higher $T_{g,org}$ values.

266   The relative humidity plays an important role in regulating SOA viscosity (Koop et al., 2011). Considering the water

267 uptake by SOA particles in the phase state estimations, the predicted geospatial patterns in the viscosity (Fig. 5a) and RH

268 (Fig. S4 in the Supplement) are very similar with each other, particularly in southern and northeastern China. SOA particles

269   are predicted to mainly be liquid or with a low viscosity ($< 10^4$ Pa s) in the southeast. Figure 5b shows the frequency of

270   liquid phase state, which is calculated as the percent time that an organic aerosol particle is in the liquid phase state during

271   the simulated period. The frequency of liquid particles varies from $\sim$ 30 % to 70 % in the southeastern China. The lowest

272   viscosity with the highest frequency of liquid particles occurs over the southern Tibetan Plateau where RH is very high (Fig.

273   S4), which is contributed by summer monsoons and regional moisture recycling (Dong et al., 2016). The SOA particles in

274   the central and northeastern China are predicted to be semi-solid, with the viscosity varied from 10^5 to 10^8 Pa s (Fig. 5a).

275   Highly viscous ($\eta > 10^8$ Pa s) or solid SOA particles are mainly found in the northwest, particularly over the northern Tibetan

276   Plateau where the ambient temperatures are lower than other areas of China (Fig. S4). The frequency of liquid SOA particles

277   in most areas with the latitude higher than 30°N is less than 20 % (Fig. 5b).

278   The simulated geospatial pattern in SOA viscosity over China agrees with previous global simulations and ambient

279   measurements. Our previous global simulations predicted a lower viscosity ($\eta < 10^3$ Pa s) in SOA particles in southeastern

280   China and a higher viscosity ($\eta > 10^8$ Pa s) in northwestern China (Shiraiwa et al., 2017; Li et al., 2020), similar to the

281   WRF-Chem simulations in this study. Interestingly, the occurrence of liquid particles over the southern Tibetan Plateau in

282   summer simulated by the WRF-Chem was not found in our previous global predictions, which was an average of five years'

283   simulations (Shiraiwa et al., 2017). The semi-solid phase state of SOA particles simulated in Beijing is consistent with both

284   particle bounce measurements (Liu et al., 2017) and the PM$_{2.5}$ phase state determined by the poke-and-flow technique (Song

285   et al., 2022). The simulated viscosity of SOA particles is 0.15 Pa s in Shenzhen, a coastal urban city in southeastern China,

286   which also agrees with the findings in the previous bounce measurements indicating that the submicron particles in

287   Shenzhen are in the liquid state (Liu et al., 2019).

288   The phase state of SOA particles is affected by ambient conditions and the particle chemical composition (Koop et al.,

289   2011). Figure 6 shows the median values of viscosity as a function of RH, T and the mass fraction of low-volatility

290   compound (SOAX with C^* of 0.1 μg m^{-3} at 298 K) calculated for selected regions in the northern China, southern China,

291   northern Qinghai-Tibet Plateau, and southern Qinghai-Tibet Plateau as specified by white boxes in Fig. 5a. There is a strong

292   inverse relationship between SOA viscosity and relative humidity with high RH ($> \sim$ 60 %) as the dominant factor

293   determining the phase state of SOA particles. When RH is lower than $\sim$ 60 %, the predicted viscosity is affected by both RH

294   and T. For example, the SOA particles occur mainly as solid over the Northern Qinghai-Tibet Plateau while occur as

295   semi-solid over the Northern China within similar RH ranges (20 % < RH < 60 %); the reason is that the ambient T over the

296   Northern Qinghai-Tibet Plateau is much lower ($\sim$ 20 K lower) than the Northern China (Fig. 6b). When RH is relatively low,

297   the viscosity of SOA particles is also influenced by particle chemical composition, i.e., the SOA particles composed of high

298   mass fractions of low volatility compounds tend to have higher viscosity values (Fig. 6c). RH is the main factor driving the

299   diurnal variations of SOA viscosity in our simulations. Figure S5 in the Supplement shows that SOA particles have higher

300   viscosity in the daytime than the nighttime as RH in the daytime is lower than the nighttime (Fig. S6). Compared to the

301 northern China, the southern China exhibits stronger diurnal variations in SOA viscosity that SOA particles occur mainly as

302 semi-solid in the daytime and liquid in the nighttime. Highly viscous or solid SOA particles are found in the northern China

303 during both daytime and nighttime (Fig. S5).

304   The bulk diffusion coefficient is an important parameter determining the mass-transport and mixing rates, which can be

305 predicted by the particle viscosity through the fractional Stokes-Einstein relation (see the Method section and the

306 Supplement). The D_b of organic molecules is predicted to be $> \sim 10^{-10}$ $cm^2 s^{-1}$ in the southern China. The highest value is

307 $\sim 10^{-5}$ $cm^2 s^{-1}$ occurring in liquid SOA particles in the southern Tibetan Plateau (Fig. 7a) because of the very low viscosity

308 simulated over this region (Fig. 5a). The D_b of organic molecules within semisolid SOA particles is $\sim 10^{-18} - 10^{-10}$ $cm^2 s^{-1}$ in

309 the central and northeastern China, and lower than $\sim 10^{-18}$ $cm^2 s^{-1}$ in highly viscous and solid particles in most areas of the

310 northwestern China. Figure 7b shows the percent time that the mixing timescale of organic molecules in 200 nm particles is

311 less than 1 h in the entire simulation period. The mixing timescale is found nearly always less than 1 h in the southeastern

312 region of the "Hu Huanyong Line". The "Hu Huanyong Line", proposed by the Chinese geographer Huanyong Hu, divides

313 China into two parts based on contrasting population densities (Hu, 1935), which was found also useful characterizing the

314 drought conditions, with the northwestern region much dryer than the southeastern region (Zeng et al., 2021). The mixing

315 timescale of organic molecules in highly viscous or solid SOA particles in the northwest of the "Hu Huanyong Line" is often

316 longer than 1 h (the frequency > 70 %), indicating that in these areas kinetic limitations of bulk diffusion should be

317 considered in SOA partitioning. Compared to the diffusion coefficients of organic molecules, the D_b of water molecules in

318 SOA particles at the surface is several orders of magnitude larger, with the values higher than 10^{-10} $cm^2 s^{-1}$ in the southeast,

319 and as low as $\sim 10^{-13}$ $cm^2 s^{-1}$ in the northwestern China (Fig. 7c). The mixing timescales of water molecules in SOA particles

320 with a diameter of 200 nm are of the order of milliseconds in the southeast and seconds in the northwest of China (Fig. S7 in

321 the Supplement), indicating that the activation of cloud condensation nuclei would not be inhibited, in agreement with our

322 previous global simulations (Shiraiwa et al., 2017).

323   Figure 8 shows the simulated $T_{g,org}$ and the phase state of SOA particles, as well as the mixing timescale of organic

324 molecules in SOA particles at 500 hPa. The $T_{g,org}$ ranges from ~ 285 K $- 295$ K, lower than the $T_{g,org}$ simulated at the surface

325 (Fig. 8a). The reason is that the mass fractions of LVOCs (SOAX with C^* of 0.1 µg m^{-3} at 298 K) at 500 hPa (Fig. S8 in the

326 Supplement) are smaller than the surface values (Fig. 4b). The low temperature at 500 hPa is favorable for SVOCs

327 partitioned into the particle phase, thus compared to the surface conditions, there is less semi-volatile vapors undergoing the

328 further gas-phase aging forming SOAX species. The percent time that an organic aerosol particle is in the liquid phase state

329 (the frequency of liquid SOA particles) at 500 hPa in the southeastern China is 20 – 35 % (Fig. 8b), which is ~ 20 % lower

330 than the surface values (Fig. 5b). In the northern China, the frequency of liquid SOA particles at 500 hPa is similar to the

331 results at the surface, which is related to the RH spatial patterns (Fig. S9 in the Supplement). The mixing timescale of

332 organic molecules in 200 nm SOA particles is frequently longer than 1 h at 500 hPa, with the frequency > 70 % in the

northern China and ~ 40 % in the southeastern China (Fig. 8c). The τ_{mix} is relatively short (the frequency of $\tau_{mix} \leq 1$ h being ~

80 %) in some areas of the southwestern China at 500 hPa, where relatively high RH could occur (Fig. S9 in the Supplement)

in the season of summer monsoon (Huang et al., 1998).

3.3 Sensitivity simulations

3.3.1 Impacts of volatility distributions on phase state estimations

The volatility and viscosity of organic aerosols are closely related (Rothfuss and Petters, 2017; Shiraiwa et al., 2017;

Champion et al., 2019; Zhang et al., 2019b; Li et al., 2020). In this section we conduct sensitivity simulations (case A, Table

1) to evaluate how the simulated volatility distributions affect the phase state estimations. The lowest C^* bin in the base case

is 0.1 μg m^{-3} at 298 K, with ΔH_{vap} of 142 kJ mol^{-1}, which does not incorporate ELVOC species at the room temperature. The

sensitivity simulation (case A) adopts the default setting in the official WRF-Chem model v3.7.1, assuming that the lowest

C^* is 0.0001 μg m^{-3} at 298 K, with ΔH_{vap} of 40 kJ mol^{-1} (Knote et al., 2015). Figure 9a shows that including these ELVOCs at

298 K with a relatively small ΔH_{vap} mainly affect the $T_{g,org}$ simulated over remote areas, e.g., the northwestern China and the

marine areas, where the simulated $T_{g,org}$ is increased by 30 – 40 K. In other regions of China, the changes in $T_{g,org}$ are less

than 25 K. Although consideration of these ELVOCs could affect the simulated $T_{g,org}$ at the surface obviously in remote areas,

i.e., the northwestern China, it does not impact the predicted frequency of the occurrence of a liquid phase state (Fig. 9b), as

in these dry areas the SOA particles are highly viscous. Including ELVOC formation at 298 K (ΔH_{vap} of 40 kJ mol^{-1}) mainly

affects the phase state estimations in areas with a moderate humidity. For example, in some areas of the southeastern China

with ~ 70 % RH, the SOA particles are predicted to be more viscous, with the frequency of a liquid phase state decreasing by

up to 12 % (Fig. 9b). These results indicate that the SOA phase state estimations in the base and sensitivity case A are

generally in agreement in the simulated episode in this study. Ambient measurements of organic aerosol volatility

distributions are still sparse over China. A recent field study showed that the ELVOCs contributed more than half to the OA

mass observed at a regional background site near the Bohai Sea (Feng et al., 2023), which resulted in an estimated viscosity

much higher than our WRF-Chem simulations. More field volatility distribution measurements should be conducted over

China to further evaluate the effects of ELVOCs and how to choose reasonable values of the enthalpy of vaporization that

would affect phase state estimations.

3.3.2 Impacts of RH and the water absorbed by inorganics on phase state estimations

RH is an important parameter affecting the phase state estimations. We perform a sensitivity calculation (case B, Table 1)

with the simulated RH increased by a factor of 10 % to compensate for the fact that the current model underestimates the

observed RH as shown in Fig. 2 and found in our previous simulations (Qu et al., 2019; Zhang et al., 2022). The increases in

simulated RH lead to more occurrence (the liquid frequency increased by 10 – 20 %) of liquid SOA particles in southeastern

China where the predicted RH is ranged mainly from 70 to 80 % (Fig. S4 in the Supplement), with very limited effects in phase state predictions in relatively dry areas, e.g., the northern China (Fig. 10a).

Besides RH, the mixing state of the organic and inorganic species in atmospheric particles also plays an important role in the phase state of ambient particles. The SOA components are assumed to be phase separated from inorganic compounds in particles in our base simulation, which is consistent to recent ambient observations showing that the phase separation with an organic-rich shell and an inorganic core was a frequent phenomenon in individual particles (diameters > 100 nm) collected over the North China Plain (Li et al., 2021a). To assess the potential effects of inorganic compounds on the phase state of ambient particles, we perform a sensitivity calculation (case C, Table 1) assuming that the organic and inorganic compounds are internally mixed in one phase. In this case the water absorbed by inorganic species can lower the particle viscosity relative to the organic fraction alone. Figure 10b shows that the water associated with inorganic species can significantly lower the viscosity over most areas of China, with the liquid frequency increased by 15 – 45 % in the southeast, and 5 – 15 % in some areas of the northeast. The effects over dry lands in the northwestern China are relatively small. Previous studies showed that at such mixing condition with one phase, on one hand, it is expected that the inorganic salts that often have lower T_g compared to SOA compounds would further lower the particle viscosity (Dette and Koop, 2015). On the other hand, the presence of divalent inorganic ions could increase the viscosity of mixed organic-inorganic particles, enabling a humidity-dependent gel phase transition through cooperative ion-molecule interactions (Richards et al., 2020). For complex mixtures of primary OA, SOA and inorganics, it was found that three distinct phases could occur (Huang et al., 2021). The impacts of the mixing state of organic and inorganic compounds on the phase state of multicomponent particles in ambient air warrant further investigations in future studies (Lilek and Zuend, 2022; Schervish and Shiraiwa, 2023).

4 Conclusions

We previously developed a new parameterization predicting the glass transition temperature of an organic compound as a function of its volatility (Li et al., 2020). Based on this new parameterization, we use the WRF-Chem model and simulate the T_g and viscosity of SOA particles over China in summer of 2018. This is the first time that spatial and temporal variations in the SOA phase state over China are investigated on a regional scale. The main conclusions are summarized below.

(1) Simulations show that T_g values of dry SOA ($T_{g,org}$) range from ~287 K to 305 K over most areas of China at the surface, consistent with our previous simulated results based on a global transport model (Shiraiwa et al., 2017). The $T_{g,org}$ is higher in the northwestern China than the southeastern China. This geospatial variation in $T_{g,org}$ is related to the simulated SOA volatility distributions that SOA particles in northwestern China have relatively low volatilities.

(2) Considering the water uptake by SOA particles, the SOA viscosity also shows a prominent geospatial gradient that highly viscous or solid SOA particles are mainly found in the northwestern China. The frequency of liquid SOA particles in most

393 areas with the latitude higher than 30°N is less than 20 %. A very large spatial variation in SOA phase state over the

394 Qinghai-Tibet Plateau was found and we recommend measurements in ambient particle phase state to be conducted over this

395 area, one of the most sensitive regions to climate change.

396 (3) The mixing timescale of organic molecules in 200 nm SOA particles is calculated based on the simulated particle

397 viscosity and the bulk diffusion coefficients of organic molecules. Calculations show that at the surface and at 500 hPa, the

398 percent time of τ_{mix} longer than 1 h is $> \sim 70$ % in the northwest of the "Hu Huanyong Line". The implication of this result is

399 that when the τ_{mix} values are greater than roughly 1 h, which is longer than the typical time step in CTMs, the instantaneous

400 equilibrium partitioning usually assumed in SOA formation simulations is subject to be re-evaluated. We recommend to test

401 the effects of kinetic partitioning considering the bulk diffusion in viscous particles on the prediction of SOA mass

402 concentrations and size distributions over the areas with long mixing timescale of organic molecules.

403 (4) The average volatility (C^*) and $T_{\text{g,org}}$ of the simulated SOA agree well with the values estimated from ambient

404 measurements of OOA volatilities at the IAP site in Beijing, where ELVOCs were not determined in the observed OOA (Xu

405 et al., 2019). The sensitivity simulation considering the formation of ELVOCs shows that compared to the base simulation,

406 the frequency of a liquid phase state does not change in most areas of the northern China. In some areas of the southeastern

407 China the SOA particles become more viscous with the percent time that a SOA particle is in the liquid phase state decreases

408 by up to 12 %. It needs more field volatility measurements to evaluate the effects of ELVOCs on OA phase state estimations

409 over China.

410 (5) Differed from the base simulation that SOA components are assumed to be phase separated from inorganic compounds in

411 particles, we conduct a sensitivity simulation assuming that the organic and inorganic compounds are internally mixed in one

412 phase. We show that the water absorbed by inorganic species has a significant impact lowering the simulated viscosity over

413 the southeastern China, with the liquid frequency increased by 15 – 45 %. Future work should consider the effects of the

414 mixing state of organic and inorganic compounds on the prediction of the phase state of multicomponent particles in ambient

415 air.

416   In summary, our simulations demonstrate the spatial distributions of the glass transition temperature and viscosity of

417 SOA particles over China on a regional scale for the first time. The further calculations of the mixing timescale of organic

418 molecules in SOA particles have an implication of the need to evaluate the effects of the phase state on predictions of SOA

419 gas-particle partitioning, and thus the SOA mass concentrations and size distributions in CTMs.

420 *Data availability.* The simulation data in this study are available upon request from the corresponding author

421 (liying-iap@mail.iap.ac.cn).

422 *Supplement.* The supplement related to this article is available on-line.

Author contributions. YL and MS designed the research. ZZ, HR, and YQ performed the WRF-Chem modeling. ZZ, YL, and HR analyzed the simulation data. WZ, WX, WH, and YS provided observation data. YL, ZZ, and MS wrote the manuscript. ZZ, YL, and HR wrote the supplement. All authors discussed the results and contributed to the article editing.

Competing interests. At least one of the (co-)authors is a member of the editorial board of Atmospheric Chemistry and Physics. The peer-review process was guided by an independent editor, and the authors have also no other competing interests to declare.

Acknowledgements. This work was supported by the National Natural Science Foundation of China (grant no. 42075110). The authors thank Qi Chen at the Peking University and Bin Zhao at the Tsinghua University for insightful suggestions on SOA volatility simulations in this work. MS thanks U.S. National Science Foundation for funding (AGS- 2246502).

Financial support. This work was supported by the National Natural Science Foundation of China (grant no. 42075110).

References

Abbatt, J. P. D., Lee, A. K. Y., and Thornton, J. A.: Quantifying trace gas uptake to tropospheric aerosol: recent advances and remaining challenges, Chem. Soc. Rev., 41, 6555-6581, https://doi.org/10.1039/C2CS35052A, 2012.

Ahmadov, R., Mckeen, S. A., Robinson, A. L., Bahreini, R., Middlebrook, A. M., De Gouw, J. A., Meagher, J., Hsie, E. Y., Edgerton, E., Shaw, S., and Trainer, M.: A volatility basis set model for summertime secondary organic aerosols over the eastern United States in 2006, J. Geophys. Res.: Atmos., 117, https://doi.org/10.1029/2011JD016831, 2012.

Angell, C. A.: Relaxation in liquids, polymers and plastic crystals — strong/fragile patterns and problems, J. Non-Cryst. Solids, 131-133, 13-31, https://doi.org/10.1016/0022-3093(91)90266-9, 1991.

Baboomian, V. J., Crescenzo, G. V., Huang, Y., Mahrt, F., Shiraiwa, M., Bertram, A. K., and Nizkorodov, S. A.: Sunlight can convert atmospheric aerosols into a glassy solid state and modify their environmental impacts, P. Natl. Acad. Sci. USA, 119, e2208121119, https://doi.org/10.1073/pnas.2208121119, 2022.

Champion, W. M., Rothfuss, N. E., Petters, M. D., and Grieshop, A. P.: Volatility and viscosity are correlated in terpene secondary organic aerosol formed in a flow reactor, Environ. Sci. Technol. Lett., 6, 513-519, https://doi.org/10.1021/acs.estlett.9b00412, 2019.

Chang, X., Zhao, B., Zheng, H., Wang, S., Cai, S., Guo, F., Gui, P., Huang, G., Wu, D., Han, L., Xing, J., Man, H., Hu, R., Liang, C., Xu, Q., Qiu, X., Ding, D., Liu, K., Han, R., Robinson, A. L., and Donahue, N. M.: Full-volatility emission framework corrects missing and underestimated secondary organic aerosol sources, One Earth, 5, 403-412, https://doi.org/10.1016/j.oneear.2022.03.015, 2022.

Dalton, A. B. and Nizkorodov, S. A.: Photochemical degradation of 4-nitrocatechol and 2,4-dinitrophenol in a sugar-glass secondary organic aerosol surrogate, Environ. Sci. Technol., 55, 14586-14594, https://doi.org/10.1021/acs.est.1c04975, 2021.

DeRieux, W. S. W., Li, Y., Lin, P., Laskin, J., Laskin, A., Bertram, A. K., Nizkorodov, S. A., and Shiraiwa, M.: Predicting the glass transition temperature and viscosity of secondary organic material using molecular composition, Atmos. Chem. Phys., 18, 6331-6351, https://doi.org/10.5194/acp-18-6331-2018, 2018.

Dette, H. P. and Koop, T.: Glass formation processes in mixed inorganic/organic aerosol particles, J. Phys. Chem. A, 119, 4552-4561, https://doi.org/10.1021/jp5106967, 2015.

Dette, H. P., Qi, M., Schröder, D. C., Godt, A., and Koop, T.: Glass-forming properties of 3-methylbutane-1,2,3-tricarboxylic acid and its mixtures with water and pinonic acid, J. Phys. Chem. A, 118, 7024-7033,

https://doi.org/10.1021/jp505910w, 2014.

Donahue, N., Robinson, A., Stanier, C., and Pandis, S.: Coupled partitioning, dilution, and chemical aging of semivolatile organics, Environ. Sci. Technol., 40, 2635-2643, https://doi.org/10.1021/es052297c, 2006.

Donahue, N. M., Epstein, S. A., Pandis, S. N., and Robinson, A. L.: A two-dimensional volatility basis set: 1. organic-aerosol mixing thermodynamics, Atmos. Chem. Phys., 11, 3303-3318, https://doi.org/10.5194/acp-11-3303-2011, 2011.

Donahue, N. M., Kroll, J. H., Pandis, S. N., and Robinson, A. L.: A two-dimensional volatility basis set – Part 2: Diagnostics of organic-aerosol evolution, Atmos. Chem. Phys., 12, 615-634, https://doi.org/10.5194/acp-12-615-2012, 2012.

Dong, W., Lin, Y., Wright, J. S., Ming, Y., Xie, Y., Wang, B., Luo, Y., Huang, W., Huang, J., Wang, L., Tian, L., Peng, Y., and Xu, F.: Summer rainfall over the southwestern Tibetan Plateau controlled by deep convection over the Indian subcontinent, Nat. Commun., 7, 10925, https://doi.org/10.1038/ncomms10925, 2016.

Duplissy, J., Decarlo, P. F., Dommen, J., Alfarra, M. R., Metzger, A., Barmpadimos, I., Prevot, A. S. H., Weingartner, E., Tritscher, T., Gysel, M., Aiken, A. C., Jimenez, J. L., Canagaratna, M. R., Worsnop, D. R., Collins, D. R., Tomlinson, J., and Baltensperger, U.: Relating hygroscopicity and composition of organic aerosol particulate matter, Atmos. Chem. Phys., 11, 1155-1165, https://doi.org/10.5194/acp-11-1155-2011, 2011.

Einstein, A.: Über die von der molekularkinetischen Theorie der Wärme geforderte Bewegung von in ruhenden Flüssigkeiten suspendierten Teilchen, 322, 549-560, https://doi.org/10.1002/andp.19053220806, 1905.

Emmons, L. K., Walters, S., Hess, P. G., Lamarque, J. F., Pfister, G. G., Fillmore, D., Granier, C., Guenther, A., Kinnison, D., Laepple, T., Orlando, J., Tie, X., Tyndall, G., Wiedinmyer, C., Baughcum, S. L., and Kloster, S.: Description and evaluation of the model for ozone and related chemical tracers, version 4 (MOZART-4), Geosci. Model Dev., 3, 43-67, https://doi.org/10.5194/gmd-3-43-2010, 2010.

Epstein, S. A., Riipinen, I., and Donahue, N. M.: A semiempirical correlation between enthalpy of vaporization and saturation concentration for organic aerosol, Environ. Sci. Technol., 44, 743-748, https://doi.org/10.1021/es902497z, 2010.

Evoy, E., Kamal, S., Patey, G. N., Martin, S. T., and Bertram, A. K.: Unified description of diffusion coefficients from small to large molecules in organic–water mixtures, J. Phys. Chem. A, 124, 2301-2308, https://doi.org/10.1021/acs.jpca.9b11271, 2020.

Evoy, E., Maclean, A. M., Rovelli, G., Li, Y., Tsimpidi, A. P., Karydis, V. A., Kamal, S., Lelieveld, J., Shiraiwa, M., Reid, J. P., and Bertram, A. K.: Predictions of diffusion rates of large organic molecules in secondary organic aerosols using the Stokes–Einstein and fractional Stokes–Einstein relations, Atmos. Chem. Phys., 19, 10073-10085, https://doi.org/10.5194/acp-19-10073-2019, 2019.

Fast, J. D., Gustafson Jr, W. I., Easter, R. C., Zaveri, R. A., Barnard, J. C., Chapman, E. G., Grell, G. A., and Peckham, S. E.: Evolution of ozone, particulates, and aerosol direct radiative forcing in the vicinity of Houston using a fully coupled meteorology-chemistry-aerosol model, J. Geophys. Res.: Atmos., 111, https://doi.org/10.1029/2005JD006721, 2006.

Feng, T., Wang, Y., Hu, W., Zhu, M., Song, W., Chen, W., Sang, Y., Fang, Z., Deng, W., Fang, H., Yu, X., Wu, C., Yuan, B., Huang, S., Shao, M., Huang, X., He, L., Lee, Y. R., Huey, L. G., Canonaco, F., Prevot, A. S. H., and Wang, X.: Impact of aging on the sources, volatility, and viscosity of organic aerosols in Chinese outflows, Atmos. Chem. Phys., 23, 611-636, https://doi.org/10.5194/acp-23-611-2023, 2023.

Fröhlich, R., Cubison, M. J., Slowik, J. G., Bukowiecki, N., Prévôt, A. S. H., Baltensperger, U., Schneider, J., Kimmel, J. R., Gonin, M., Rohner, U., Worsnop, D. R., and Jayne, J. T.: The ToF-ACSM: a portable aerosol chemical speciation monitor with TOFMS detection, Atmos. Meas. Tech., 6, 3225-3241, https://doi.org/10.5194/amt-6-3225-2013, 2013.

Galeazzo, T. and Shiraiwa, M.: Predicting glass transition temperature and melting point of organic compounds via machine learning and molecular embeddings, Environ. Sci.: Atmos., https://doi.org/10.1039/D1EA00090J, 2022.

Gervasi, N. R., Topping, D. O., and Zuend, A.: A predictive group-contribution model for the viscosity of aqueous organic aerosol, Atmos. Chem. Phys., 20, 2987-3008, https://doi.org/10.5194/acp-20-2987-2020, 2020.

Gordon, M. and Taylor, J. S.: Ideal copolymers and the second-order transitions of synthetic rubbers. i. non-crystalline copolymers, J. Appl. Chem., 2, 493-500, https://doi.org/10.1002/jctb.5010020901, 1952.

Grell, G. A., Peckham, S. E., Schmitz, R., Mckeen, S. A., Frost, G., Skamarock, W. C., and Eder, B.: Fully coupled "online"

chemistry within the WRF model, Atmos. Environ., 39, 6957-6975, https://doi.org/10.1016/j.atmosenv.2005.04.027, 2005.

Guenther, A. B., Jiang, X., Heald, C. L., Sakulyanontvittaya, T., Duhl, T., Emmons, L. K., and Wang, X.: The Model of Emissions of Gases and Aerosols from Nature version 2.1 (MEGAN2.1): an extended and updated framework for modeling biogenic emissions, Geosci. Model Dev., 5, 1471-1492, https://doi.org/10.5194/gmd-5-1471-2012, 2012.

Gunthe, S. S., King, S. M., Rose, D., Chen, Q., Roldin, P., Farmer, D. K., Jimenez, J. L., Artaxo, P., Andreae, M. O., Martin, S. T., and Pöschl, U.: Cloud condensation nuclei in pristine tropical rainforest air of Amazonia: size-resolved measurements and modeling of atmospheric aerosol composition and CCN activity, Atmos. Chem. Phys., 9, 7551-7575, https://doi.org/10.5194/acp-9-7551-2009, 2009.

He, Y., Akherati, A., Nah, T., Ng, N. L., Garofalo, L. A., Farmer, D. K., Shiraiwa, M., Zaveri, R. A., Cappa, C. D., Pierce, J. R., and Jathar, S. H.: Particle size distribution dynamics can help constrain the phase state of secondary organic aerosol, Environ. Sci. Technol., 55, 1466-1476, https://doi.org/10.1021/acs.est.0c05796, 2021.

Hu, H.: The distribution of China's population, Acta Geogr. Sin., 2, 33-73, https://doi.org/10.11821/xb193502002, 1935.

Huang, R., Zhang, Z., Huang, G., and Ren, B.: Characteristics of the water vapor transport in east Asian monsoon region and its differences from that of south Asian monsoon region in summer, Chinese J. Atmospheric Sci., 22, 368-379, https://doi.org/10.3878/j.issn.1006-9895.2003.19204, 1998.

Huang, Y., Mahrt, F., Xu, S., Shiraiwa, M., Zuend, A., and Bertram, A. K.: Coexistence of three liquid phases in individual atmospheric aerosol particles, P. Natl. Acad. Sci. USA, 118, e2102512118, https://doi.org/10.1073/pnas.2102512118, 2021.

Jathar, S. H., Cappa, C. D., He, Y., Pierce, J. R., Chuang, W., Bilsback, K. R., Seinfeld, J. H., Zaveri, R. A., and Shrivastava, M.: A computationally efficient model to represent the chemistry, thermodynamics, and microphysics of secondary organic aerosols (simpleSOM): model development and application to α-pinene SOA, Environ. Sci.: Atmos., 1, 372-394, https://doi.org/10.1039/D1EA00014D, 2021.

Jimenez, J. L., Canagaratna, M. R., Donahue, N. M., Prevot, A. S. H., Zhang, Q., Kroll, J. H., Decarlo, P. F., Allan, J. D., Coe, H., Ng, N. L., Aiken, A. C., Docherty, K. S., Ulbrich, I. M., Grieshop, A. P., Robinson, A. L., Duplissy, J., Smith, J. D., Wilson, K. R., Lanz, V. A., Hueglin, C., Sun, Y. L., Tian, J., Laaksonen, A., Raatikainen, T., Rautiainen, J., Vaattovaara, P., Ehn, M., Kulmala, M., Tomlinson, J. M., Collins, D. R., Cubison, M. J., Dunlea, J., Huffman, J. A., Onasch, T. B., Alfarra, M. R., Williams, P. I., Bower, K., Kondo, Y., Schneider, J., Drewnick, F., Borrmann, S., Weimer, S., Demerjian, K., Salcedo, D., Cottrell, L., Griffin, R., Takami, A., Miyoshi, T., Hatakeyama, S., Shimono, A., Sun, J. Y., Zhang, Y. M., Dzepina, K., Kimmel, J. R., Sueper, D., Jayne, J. T., Herndon, S. C., Trimborn, A. M., Williams, L. R., Wood, E. C., Middlebrook, A. M., Kolb, C. E., Baltensperger, U., and Worsnop, D. R.: Evolution of organic aerosols in the atmosphere, Science, 326, 1525, https://doi.org/10.1126/science.1180353, 2009.

Kanakidou, M., Seinfeld, J. H., Pandis, S. N., Barnes, I., Dentener, F. J., Facchini, M. C., Van Dingenen, R., Ervens, B., Nenes, A., Nielsen, C. J., Swietlicki, E., Putaud, J. P., Balkanski, Y., Fuzzi, S., Horth, J., Moortgat, G. K., Winterhalter, R., Myhre, C. E. L., Tsigaridis, K., Vignati, E., Stephanou, E. G., and Wilson, J.: Organic aerosol and global climate modelling: a review, Atmos. Chem. Phys., 5, 1053-1123, https://doi.org/10.5194/acp-5-1053-2005, 2005.

Karnezi, E., Riipinen, I., and Pandis, S. N.: Measuring the atmospheric organic aerosol volatility distribution: a theoretical analysis, Atmos. Meas. Tech., 7, 2953-2965, https://doi.org/10.5194/amt-7-2953-2014, 2014.

Knopf, D. A. and Alpert, P. A.: Atmospheric ice nucleation, Nat. Rev. Phys., 5, 203-217, https://doi.org/10.1038/s42254-023-00570-7, 2023.

Knote, C., Hodzic, A., and Jimenez, J. L.: The effect of dry and wet deposition of condensable vapors on secondary organic aerosols concentrations over the continental US, Atmos. Chem. Phys., 15, 1-18, https://doi.org/10.5194/acp-15-1-2015, 2015.

Kohl, I., Bachmann, L., Hallbrucker, A., Mayer, E., and Loerting, T.: Liquid-like relaxation in hyperquenched water at ≤140 K, Phys. Chem. Chem. Phys., 7, 3210-3220, https://doi.org/10.1039/B507651J, 2005.

Koop, T., Bookhold, J., Shiraiwa, M., and Pöschl, U.: Glass transition and phase state of organic compounds: dependency on molecular properties and implications for secondary organic aerosols in the atmosphere, Phys. Chem. Chem. Phys., 13,

19238-19255, https://doi.org/10.1039/C1CP22617G, 2011.

Kuwata, M. and Martin, S. T.: Phase of atmospheric secondary organic material affects its reactivity, P. Natl. Acad. Sci. USA, 109, 17354-17359, https://doi.org/10.1073/pnas.1209071109, 2012.

Lane, T. E., Donahue, N. M., and Pandis, S. N.: Effect of NOx on secondary organic aerosol concentrations, Environ. Sci. Technol., 42, 6022-6027, https://doi.org/10.1021/es703225a, 2008a.

Lane, T. E., Donahue, N. M., and Pandis, S. N.: Simulating secondary organic aerosol formation using the volatility basis-set approach in a chemical transport model, Atmos. Environ., 42, 7439-7451, https://doi.org/10.1016/j.atmosenv.2008.06.026, 2008b.

Li, J., Han, Z., Wu, J., Tao, J., Li, J., Sun, Y., Liang, L., Liang, M., and Wang, Q. G.: Secondary organic aerosol formation and source contributions over east China in summertime, Environ. Pollut., 306, 119383, https://doi.org/10.1016/j.envpol.2022.119383, 2022.

Li, M., Zhang, Q., Kurokawa, J. I., Woo, J. H., He, K., Lu, Z., Ohara, T., Song, Y., Streets, D. G., Carmichael, G. R., Cheng, Y., Hong, C., Huo, H., Jiang, X., Kang, S., Liu, F., Su, H., and Zheng, B.: MIX: a mosaic Asian anthropogenic emission inventory under the international collaboration framework of the MICS-Asia and HTAP, Atmos. Chem. Phys., 17, 935-963, https://doi.org/10.5194/acp-17-935-2017, 2017.

Li, W., Liu, L., Zhang, J., Xu, L., Wang, Y., Sun, Y., and Shi, Z.: Microscopic evidence for phase separation of organic species and inorganic salts in fine ambient aerosol particles, Environ. Sci. Technol., 55, 2234-2242, https://doi.org/10.1021/acs.est.0c02333, 2021a.

Li, Y. and Shiraiwa, M.: Timescales of secondary organic aerosols to reach equilibrium at various temperatures and relative humidities, Atmos. Chem. Phys., 19, 5959-5971, https://doi.org/10.5194/acp-19-5959-2019, 2019.

Li, Y., An, J., and Gultepe, I.: Effects of additional HONO sources on visibility over the North China Plain, Adv. Atmos. Sci., 31, 1221-1232, https://doi.org/10.1007/s00376-014-4019-1, 2014.

Li, Y., Carlton, A. G., and Shiraiwa, M.: Diurnal and seasonal variations in the phase state of secondary organic aerosol material over the contiguous US simulated in CMAQ, ACS Earth Space Chem., 5, 1971-1982, https://doi.org/10.1021/acsearthspacechem.1c00094, 2021b.

Li, Y., Day, D. A., Stark, H., Jimenez, J. L., and Shiraiwa, M.: Predictions of the glass transition temperature and viscosity of organic aerosols from volatility distributions, Atmos. Chem. Phys., 20, 8103-8122, https://doi.org/10.5194/acp-20-8103-2020, 2020.

Li, Y., An, J., Min, M., Zhang, W., Wang, F., and Xie, P.: Impacts of HONO sources on the air quality in Beijing, Tianjin and Hebei Province of China, Atmos. Environ., 45, 4735-4744, https://doi.org/10.1016/j.atmosenv.2011.04.086, 2011.

Li, Y., An, J., Kajino, M., Gultepe, I., Chen, Y., Song, T., and Xin, J.: Impacts of additional HONO sources on O_3 and $PM_{2.5}$ chemical coupling and control strategies in the Beijing–Tianjin–Hebei region of China, Tellus B, 67, 23930, https://doi.org/10.3402/tellusb.v67.23930, 2015.

Li, Z., Xu, W., Zhou, W., Lei, L., Sun, J., You, B., Wang, Z., and Sun, Y.: Insights into the compositional differences of PM_1 and $PM_{2.5}$ from aerosol mass spectrometer measurements in Beijing, China, Atmos. Environ., 301, 119709, https://doi.org/10.1016/j.atmosenv.2023.119709, 2023.

Lilek, J. and Zuend, A.: A predictive viscosity model for aqueous electrolytes and mixed organic–inorganic aerosol phases, Atmos. Chem. Phys., 22, 3203-3233, https://doi.org/10.5194/acp-22-3203-2022, 2022.

Liu, P., Li, Y. J., Wang, Y., Bateman, A. P., Zhang, Y., Gong, Z., Bertram, A. K., and Martin, S. T.: Highly viscous states affect the browning of atmospheric organic particulate matter, ACS Cent. Sci., 4, 207-215, https://doi.org/10.1021/acscentsci.7b00452, 2018.

Liu, Y., Wu, Z., Wang, Y., Xiao, Y., Gu, F., Zheng, J., Tan, T., Shang, D., Wu, Y., Zeng, L., Hu, M., Bateman, A. P., and Martin, S. T.: Submicrometer particles are in the liquid state during heavy haze episodes in the urban atmosphere of Beijing, China, Environ. Sci. Technol. Lett., 4, 427-432, https://doi.org/10.1021/acs.estlett.7b00352, 2017.

Liu, Y., Meng, X., Wu, Z., Huang, D., Wang, H., Chen, J., Chen, J., Zong, T., Fang, X., Tan, T., Zhao, G., Chen, S., Zeng, L., Guo, S., Huang, X., He, L., Zeng, L., and Hu, M.: The particle phase state during the biomass burning events, Sci. Total Environ., 792, 148035, https://doi.org/10.1016/j.scitotenv.2021.148035, 2021.

Maclean, A. M., Butenhoff, C. L., Grayson, J. W., Barsanti, K., Jimenez, J. L., and Bertram, A. K.: Mixing times of organic molecules within secondary organic aerosol particles: a global planetary boundary layer perspective, Atmos. Chem. Phys., 17, 13037-13048, https://doi.org/10.5194/acp-17-13037-2017, 2017.

Maclean, A. M., Li, Y., Crescenzo, G. V., Smith, N. R., Karydis, V. A., Tsimpidi, A. P., Butenhoff, C. L., Faiola, C. L., Lelieveld, J., Nizkorodov, S. A., Shiraiwa, M., and Bertram, A. K.: Global distribution of the phase state and mixing times within secondary organic aerosol particles in the troposphere based on room-temperature viscosity measurements, ACS Earth Space Chem., 5, 3458-3473, https://doi.org/10.1021/acsearthspacechem.1c00296, 2021.

Marshall, F. H., Berkemeier, T., Shiraiwa, M., Nandy, L., Ohm, P. B., Dutcher, C. S., and Reid, J. P.: Influence of particle viscosity on mass transfer and heterogeneous ozonolysis kinetics in aqueous–sucrose–maleic acid aerosol, Phys. Chem. Chem. Phys., 20, 15560-15573, https://doi.org/10.1039/C8CP01666F, 2018.

Meng, X., Wu, Z., Guo, S., Wang, H., Liu, K., Zong, T., Liu, Y., Zhang, W., Zhang, Z., Chen, S., Zeng, L., Hallquist, M., Shuai, S., and Hu, M.: Humidity-dependent phase state of gasoline vehicle emission-related aerosols, Environ. Sci. Technol., 55, 832-841, https://doi.org/10.1021/acs.est.0c05478, 2021.

Miao, R., Chen, Q., Shrivastava, M., Chen, Y., Zhang, L., Hu, J., Zheng, Y., and Liao, K.: Process-based and observation-constrained SOA simulations in China: the role of semivolatile and intermediate-volatility organic compounds and OH levels, Atmos. Chem. Phys., 21, 16183-16201, https://doi.org/10.5194/acp-21-16183-2021, 2021.

Mikhailov, E., Vlasenko, S., Martin, S. T., Koop, T., and Pöschl, U.: Amorphous and crystalline aerosol particles interacting with water vapor: conceptual framework and experimental evidence for restructuring, phase transitions and kinetic limitations, Atmos. Chem. Phys., 9, 9491-9522, https://doi.org/10.5194/acp-9-9491-2009, 2009.

Murphy, B. N. and Pandis, S. N.: Simulating the formation of semivolatile primary and secondary organic aerosol in a regional chemical transport model, Environ. Sci. Technol., 43, 4722-4728, https://doi.org/10.1021/es803168a, 2009.

Pankow, J. F.: An absorption model of gas/particle partitioning of organic compounds in the atmosphere, Atmos. Environ., 28, 185-188, https://doi.org/10.1016/1352-2310(94)90093-0, 1994.

Petters, M. D. and Kreidenweis, S. M.: A single parameter representation of hygroscopic growth and cloud condensation nucleus activity, Atmos. Chem. Phys., 7, 1961-1971, https://doi.org/10.5194/acp-7-1961-2007, 2007.

Pöschl, U. and Shiraiwa, M.: Multiphase chemistry at the atmosphere–biosphere interface influencing climate and public health in the anthropocene, Chem. Rev., 115, 4440-4475, https://doi.org/10.1021/cr500487s, 2015.

Preston, T. C. and Zuend, A.: Equilibrium times in viscous and viscoelastic aerosol particles, Environ. Sci.: Atmos., https://doi.org/10.1039/D2EA00065B, 2022.

Price, H. C., Mattsson, J., and Murray, B. J.: Sucrose diffusion in aqueous solution, Phys. Chem. Chem. Phys., 18, 19207-19216, https://doi.org/10.1039/C6CP03238A, 2016.

Qu, Y., Chen, Y., Liu, X., Zhang, J., Guo, Y., and An, J.: Seasonal effects of additional HONO sources and the heterogeneous reactions of N_2O_5 on nitrate in the North China Plain, Sci. Total Environ., 690, 97-107, https://doi.org/10.1016/j.scitotenv.2019.06.436, 2019.

Rasool, Q. Z., Shrivastava, M., Liu, Y., Gaudet, B., and Zhao, B.: Modeling the Impact of the Organic Aerosol Phase State on Multiphase OH Reactive Uptake Kinetics and the Resultant Heterogeneous Oxidation Timescale of Organic Aerosol in the Amazon Rainforest, ACS Earth Space Chem., https://doi.org/10.1021/acsearthspacechem.2c00366, 2023.

Rasool, Q. Z., Shrivastava, M., Octaviani, M., Zhao, B., Gaudet, B., and Liu, Y.: Modeling volatility-based aerosol phase state predictions in the Amazon Rainforest, ACS Earth Space Chem., 5, 2910-2924, https://doi.org/10.1021/acsearthspacechem.1c00255, 2021.

Reid, J. P., Bertram, A. K., Topping, D. O., Laskin, A., Martin, S. T., Petters, M. D., Pope, F. D., and Rovelli, G.: The viscosity of atmospherically relevant organic particles, Nat. Commun., 9, 956, https://doi.org/10.1038/s41467-018-03027-z, 2018.

Richards, D. S., Trobaugh, K. L., Hajek-Herrera, J., Price, C. L., Sheldon, C. S., Davies, J. F., and Davis, R. D.: Ion-molecule interactions enable unexpected phase transitions in organic-inorganic aerosol, Sci. Adv., 6, eabb5643, https://doi.org/10.1126/sciadv.abb5643, 2020.

Riipinen, I., Pierce, J. R., Donahue, N. M., and Pandis, S. N.: Equilibration time scales of organic aerosol inside

thermodenuders: Evaporation kinetics versus thermodynamics, Atmos. Environ., 44, 597-607, https://doi.org/10.1016/j.atmosenv.2009.11.022, 2010.

Roldin, P., Eriksson, A. C., Nordin, E. Z., Hermansson, E., Mogensen, D., Rusanen, A., Boy, M., Swietlicki, E., Svenningsson, B., Zelenyuk, A., and Pagels, J.: Modelling non-equilibrium secondary organic aerosol formation and evaporation with the aerosol dynamics, gas- and particle-phase chemistry kinetic multilayer model ADCHAM, Atmos. Chem. Phys., 14, 7953-7993, https://doi.org/10.5194/acp-14-7953-2014, 2014.

Rothfuss, N. E. and Petters, M. D.: Influence of functional groups on the viscosity of organic aerosol, Environ. Sci. Technol., 51, 271-279, https://doi.org/10.1021/acs.est.6b04478, 2017.

Schervish, M. and Shiraiwa, M.: Impact of phase state and non-ideal mixing on equilibration timescales of secondary organic aerosol partitioning, Atmos. Chem. Phys., 23, 221-233, https://doi.org/10.5194/acp-23-221-2023, 2023.

Schmedding, R., Rasool, Q. Z., Zhang, Y., Pye, H. O. T., Zhang, H., Chen, Y., Surratt, J. D., Lopez-Hilfiker, F. D., Thornton, J. A., Goldstein, A. H., and Vizuete, W.: Predicting secondary organic aerosol phase state and viscosity and its effect on multiphase chemistry in a regional-scale air quality model, Atmos. Chem. Phys., 20, 8201-8225, https://doi.org/10.5194/acp-20-8201-2020, 2020.

Seinfeld, J. H. and Pandis, S. N.: Atmospheric chemistry and physics: from air pollution to climate change, John Wiley & Sons, 2016.

Shiraiwa, M. and Pöschl, U.: Mass accommodation and gas–particle partitioning in secondary organic aerosols: dependence on diffusivity, volatility, particle-phase reactions, and penetration depth, Atmos. Chem. Phys., 21, 1565-1580, https://doi.org/10.5194/acp-21-1565-2021, 2021.

Shiraiwa, M. and Seinfeld, J. H.: Equilibration timescale of atmospheric secondary organic aerosol partitioning, Geophys. Res. Lett., 39, https://doi.org/10.1029/2012GL054008, 2012.

Shiraiwa, M., Yee, L. D., Schilling, K. A., Loza, C. L., Craven, J. S., Zuend, A., Ziemann, P. J., and Seinfeld, J. H.: Size distribution dynamics reveal particle-phase chemistry in organic aerosol formation, P. Natl. Acad. Sci. USA, 110, 11746, https://doi.org/10.1073/pnas.1307501110, 2013.

Shiraiwa, M., Li, Y., Tsimpidi, A. P., Karydis, V. A., Berkemeier, T., Pandis, S. N., Lelieveld, J., Koop, T., and Pöschl, U.: Global distribution of particle phase state in atmospheric secondary organic aerosols, Nat. Commun., 8, 15002, https://doi.org/10.1038/ncomms15002, 2017.

Shrivastava, M., Fast, J., Easter, R., Gustafson Jr, W. I., Zaveri, R. A., Jimenez, J. L., Saide, P., and Hodzic, A.: Modeling organic aerosols in a megacity: comparison of simple and complex representations of the volatility basis set approach, Atmos. Chem. Phys., 11, 6639-6662, https://doi.org/10.5194/acp-11-6639-2011, 2011.

Shrivastava, M., Rasool, Q. Z., Zhao, B., Octaviani, M., Zaveri, R. A., Zelenyuk, A., Gaudet, B., Liu, Y., Shilling, J. E., Schneider, J., Schulz, C., Zöger, M., Martin, S. T., Ye, J., Guenther, A., Souza, R. F., Wendisch, M., and Pöschl, U.: Tight coupling of surface and in-plant biochemistry and convection governs key fine particulate components over the Amazon Rainforest, ACS Earth Space Chem., 6, 380-390, https://doi.org/10.1021/acsearthspacechem.1c00356, 2022.

Shrivastava, M., Cappa, C. D., Fan, J., Goldstein, A. H., Guenther, A. B., Jimenez, J. L., Kuang, C., Laskin, A., Martin, S. T., Ng, N. L., Petaja, T., Pierce, J. R., Rasch, P. J., Roldin, P., Seinfeld, J. H., Shilling, J., Smith, J. N., Thornton, J. A., Volkamer, R., Wang, J., Worsnop, D. R., Zaveri, R. A., Zelenyuk, A., and Zhang, Q.: Recent advances in understanding secondary organic aerosol: implications for global climate forcing, Rev. Geophys., 55, 509-559, https://doi.org/10.1002/2016RG000540, 2017.

Song, M., Jeong, R., Kim, D., Qiu, Y., Meng, X., Wu, Z., Zuend, A., Ha, Y., Kim, C., Kim, H., Gaikwad, S., Jang, K.-S., Lee, J. Y., and Ahn, J.: Comparison of phase states of $PM_{2.5}$ over megacities, Seoul and Beijing, and their implications on particle size distribution, Environ. Sci. Technol., https://doi.org/10.1021/acs.est.2c06377, 2022.

Song, Y. C., Haddrell, A. E., Bzdek, B. R., Reid, J. P., Bannan, T., Topping, D. O., Percival, C., and Cai, C.: Measurements and predictions of binary component aerosol particle viscosity, J. Phys. Chem. A, 120, 8123-8137, https://doi.org/10.1021/acs.jpca.6b07835, 2016.

Tan, W., Li, C., Liu, Y., Meng, X., Wu, Z., Kang, L., and Zhu, T.: Potential of polarization lidar to profile the urban aerosol phase state during haze episodes, Environ. Sci. Technol. Lett., 7, 54-59, https://doi.org/10.1021/acs.estlett.9b00695,

2020.

Tong, Y.-K., Liu, Y., Meng, X., Wang, J., Zhao, D., Wu, Z., and Ye, A.: Relative humidity-dependent viscosity of single quasi aerosol particle and possible implications for atmospheric aerosol chemistry, Phys. Chem. Chem. Phys., https://doi.org/10.1039/D2CP00740A, 2022.

Wu, Z. J., Poulain, L., Henning, S., Dieckmann, K., Birmili, W., Merkel, M., Van Pinxteren, D., Spindler, G., Müller, K., Stratmann, F., Herrmann, H., and Wiedensohler, A.: Relating particle hygroscopicity and CCN activity to chemical composition during the HCCT-2010 field campaign, Atmos. Chem. Phys., 13, 7983-7996, https://doi.org/10.5194/acp-13-7983-2013, 2013.

Xu, W., Xie, C., Karnezi, E., Zhang, Q., Wang, J., Pandis, S. N., Ge, X., Zhang, J., An, J., Wang, Q., Zhao, J., Du, W., Qiu, Y., Zhou, W., He, Y., Li, Y., Li, J., Fu, P., Wang, Z., Worsnop, D. R., and Sun, Y.: Summertime aerosol volatility measurements in Beijing, China, Atmos. Chem. Phys., 19, 10205-10216, https://doi.org/10.5194/acp-19-10205-2019, 2019.

Zaveri, R. A., Easter, R. C., Fast, J. D., and Peters, L. K.: Model for Simulating Aerosol Interactions and Chemistry (MOSAIC), J. Geophys. Res.: Atmos., 113, https://doi.org/10.1029/2007JD008782, 2008.

Zaveri, R. A., Easter, R. C., Shilling, J. E., and Seinfeld, J. H.: Modeling kinetic partitioning of secondary organic aerosol and size distribution dynamics: representing effects of volatility, phase state, and particle-phase reaction, Atmos. Chem. Phys., 14, 5153-5181, https://doi.org/10.5194/acp-14-5153-2014, 2014.

Zaveri, R. A., Shilling, J. E., Zelenyuk, A., Zawadowicz, M. A., Suski, K., China, S., Bell, D. M., Veghte, D., and Laskin, A.: Particle-phase diffusion modulates partitioning of semivolatile organic compounds to aged secondary organic aerosol, Environ. Sci. Technol., 54, 2595-2605, https://doi.org/10.1021/acs.est.9b05514, 2020.

Zaveri, R. A., Wang, J., Fan, J., Zhang, Y., Shilling, J. E., Zelenyuk, A., Mei, F., Newsom, R., Pekour, M., Tomlinson, J., Comstock, J. M., Shrivastava, M., Fortner, E., Machado, L. a. T., Artaxo, P., and Martin, S. T.: Rapid growth of anthropogenic organic nanoparticles greatly alters cloud life cycle in the Amazon rainforest, Sci. Adv., 8, eabj0329, https://doi.org/10.1126/sciadv.abj0329, 2022.

Zaveri, R. A., Shilling, J. E., Zelenyuk, A., Liu, J., Bell, D. M., D'ambro, E. L., Gaston, C. J., Thornton, J. A., Laskin, A., Lin, P., Wilson, J., Easter, R. C., Wang, J., Bertram, A. K., Martin, S. T., Seinfeld, J. H., and Worsnop, D. R.: Growth kinetics and size distribution dynamics of viscous secondary organic aerosol, Environ. Sci. Technol., 52, 1191-1199, https://doi.org/10.1021/acs.est.7b04623, 2018.

Zeng, P., Sun, F., Liu, Y., Wang, Y., Li, G., and Che, Y.: Mapping future droughts under global warming across China: a combined multi-timescale meteorological drought index and SOM-Kmeans approach, Weather Clim. Extreme, 31, 100304, https://doi.org/10.1016/j.wace.2021.100304, 2021.

Zhang, J., Lian, C., Wang, W., Ge, M., Guo, Y., Ran, H., Zhang, Y., Zheng, F., Fan, X., Yan, C., Daellenbach, K. R., Liu, Y., Kulmala, M., and An, J.: Amplified role of potential HONO sources in O_3 formation in North China Plain during autumn haze aggravating processes, Atmos. Chem. Phys., 22, 3275-3302, https://doi.org/10.5194/acp-22-3275-2022, 2022.

Zhang, Y., Chen, Y., Lei, Z., Olson, N. E., Riva, M., Koss, A. R., Zhang, Z., Gold, A., Jayne, J. T., Worsnop, D. R., Onasch, T. B., Kroll, J. H., Turpin, B. J., Ault, A. P., and Surratt, J. D.: Joint impacts of acidity and viscosity on the formation of secondary organic aerosol from isoprene epoxydiols (IEPOX) in phase separated particles, ACS Earth Space Chem., 3, 2646-2658, https://doi.org/10.1021/acsearthspacechem.9b00209, 2019a.

Zhang, Y., Nichman, L., Spencer, P., Jung, J. I., Lee, A., Heffernan, B. K., Gold, A., Zhang, Z., Chen, Y., Canagaratna, M. R., Jayne, J. T., Worsnop, D. R., Onasch, T. B., Surratt, J. D., Chandler, D., Davidovits, P., and Kolb, C. E.: The cooling rate- and volatility-dependent glass-forming properties of organic aerosols measured by broadband dielectric spectroscopy, Environ. Sci. Technol., 53, 12366-12378, https://doi.org/10.1021/acs.est.9b03317, 2019b.

Zheng, B., Tong, D., Li, M., Liu, F., Hong, C., Geng, G., Li, H., Li, X., Peng, L., Qi, J., Yan, L., Zhang, Y., Zhao, H., Zheng, Y., He, K., and Zhang, Q.: Trends in China's anthropogenic emissions since 2010 as the consequence of clean air actions, Atmos. Chem. Phys., 18, 14095-14111, https://doi.org/10.5194/acp-18-14095-2018, 2018.

Ziemann, P. J. and Atkinson, R.: Kinetics, products, and mechanisms of secondary organic aerosol formation, Chem. Soc.

743   Rev., 41, 6582-6605, https://doi.org/10.1039/C2CS35122F, 2012.

744

745

746

747

748

749

750

751

752

753

754

755

756

757

758

759

760

761

762

763

764

765

766

767

768

769

770

771 **Table 1.** Sensitivity calculations for evaluating the effects of simulated SOA volatility distributions (sensitivity case A), RH (sensitivity

772 case B) and the water absorbed by inorganic components (sensitivity case C) on viscosity estimations.

773

Cases	C^* at 298 K and ΔH_{vap} in each volatility bin	The liquid water content considered in viscosity estimations	RH
Base case	0.1, 1, 10, 100, and 1000 µg m^{-3} with ΔH_{vap} of 142, 131, 120, 109, and 98 kJ mol^{-1}	water absorbed by SOA particles with the assumption that SOA particles are externally mixed with inorganics	RH simulated by WRF-Chem
Sensitivity case A	0.0001, 1, 10, 100, and 1000 µg m^{-3} with ΔH_{vap} of 40, 131, 120, 109, and 98 kJ mol^{-1}	water absorbed by SOA particles with the assumption that SOA particles are externally mixed with inorganics	RH simulated by WRF-Chem
Sensitivity case B	0.1, 1, 10, 100, and 1000 µg m^{-3} with ΔH_{vap} of 142, 131, 120, 109, and 98 kJ mol^{-1}	water absorbed by SOA particles with the assumption that SOA particles are externally mixed with inorganics	RH simulated by WRF-Chem increased by a factor of 10%
Sensitivity case C	0.1, 1, 10, 100, and 1000 µg m^{-3} with ΔH_{vap} of 142, 131, 120, 109, and 98 kJ mol^{-1}	water absorbed by both SOA particles and inorganic components with the assumption that SOA particles are internally mixed with inorganics	RH simulated by WRF-Chem

774
775
776
777
778
779
780
781
782
783
784
785
786
787
788
789
790
791
792
793
794
795
796
797
798
799
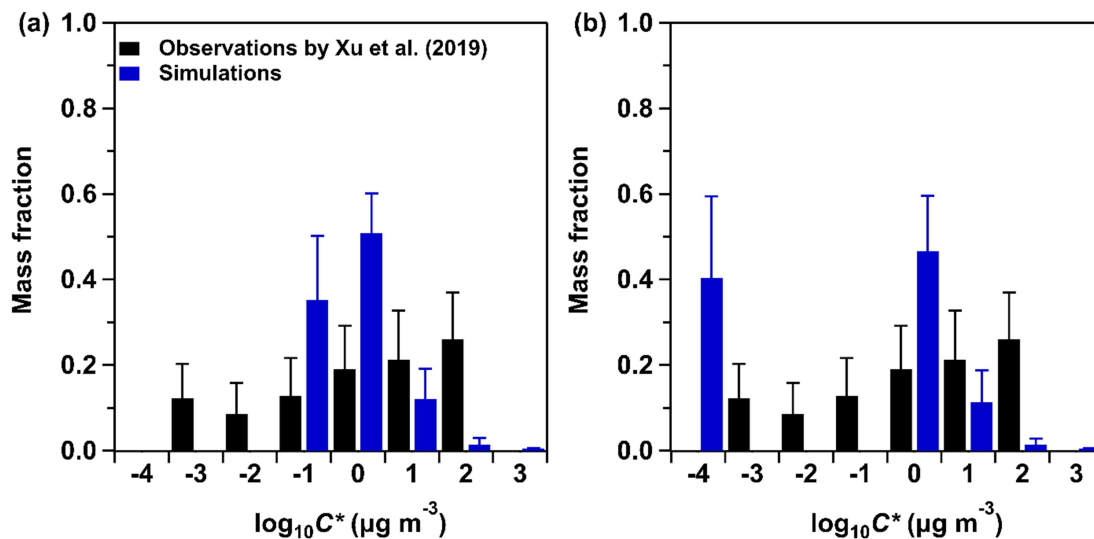
Figure 1. Comparison of the average volatility distributions of observed OOA and simulated SOA at the IAP site during 20 May – 23 June 2018. The black bars represent the volatility distributions of observed OOA adopted from Xu et al. (2019). The blue bars represent the volatility distributions of SOA simulated by WRF-Chem, with five C^* bins set to be 0.1, 1, 10, 100, and 1000 μg m^{-3} at 298 K in (a), and 0.0001, 1, 10, 100, and 1000 μg m^{-3} at 298 K in (b). The blue error bars represent the one standard deviation.
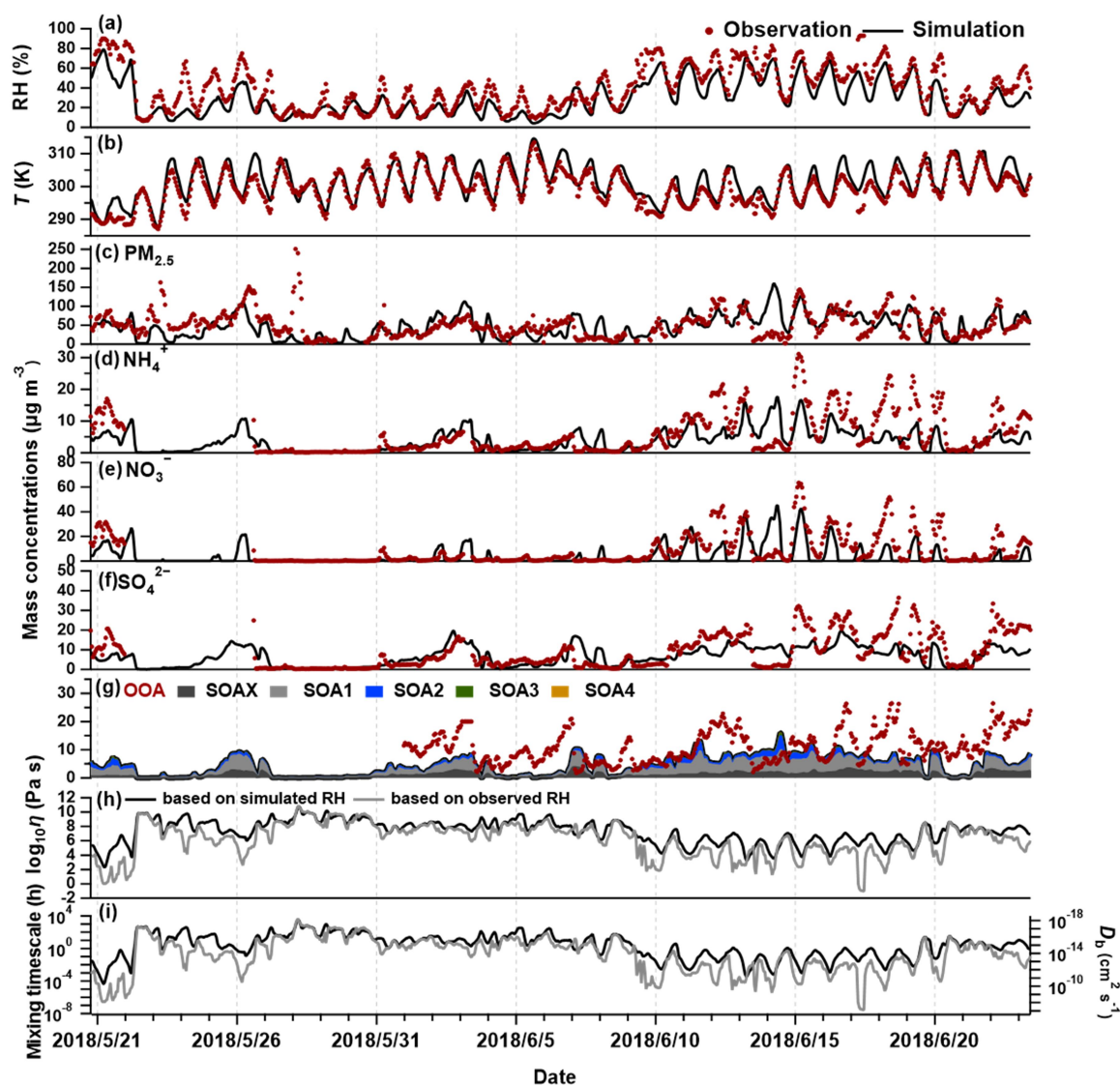
Figure 2. Observations and simulations of temporal variations of (a) RH, (b) T, (c) $PM_{2.5}$ concentrations, (d) NH_4^+ concentrations, (e) NO_3^- concentrations, and (f) SO_4^{2-} concentrations at the IAP site. (g) Observed OOA concentrations (red dots) and simulated SOA concentrations, with SOAX, SOA1, SOA2, SOA3, and SOA4 represent the SOA with C^* of 0.1, 1, 10, 100, and 1000 μg m^{-3} at 298 K, respectively. (h) SOA viscosity, and (i) bulk diffusion coefficients and mixing timescale of organic molecules within 200 nm SOA particles calculated using the RH simulated by the WRF-Chem model or the RH observed at the IAP site.
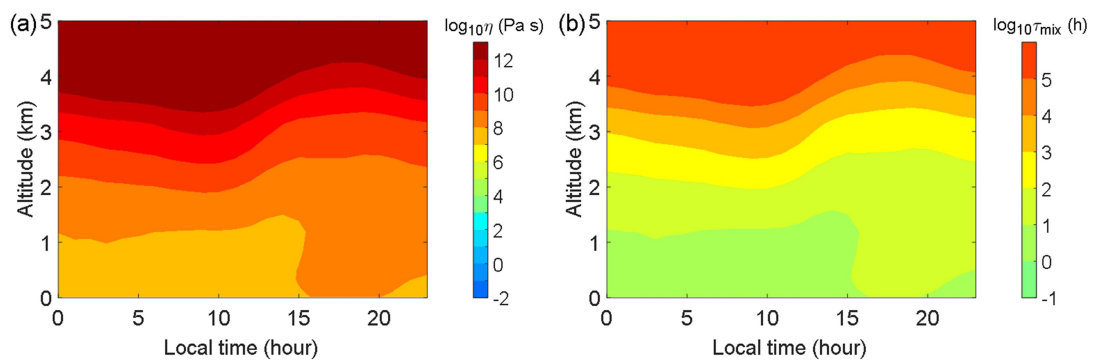
Figure 3. Median diurnal and vertical profiles of estimated (a) SOA viscosity and (b) mixing timescales for organic molecules within 200 nm SOA particles at the IAP site during May 20 – June 23 in 2018. Note: altitude is approximate and estimated from WRF pressure layers.
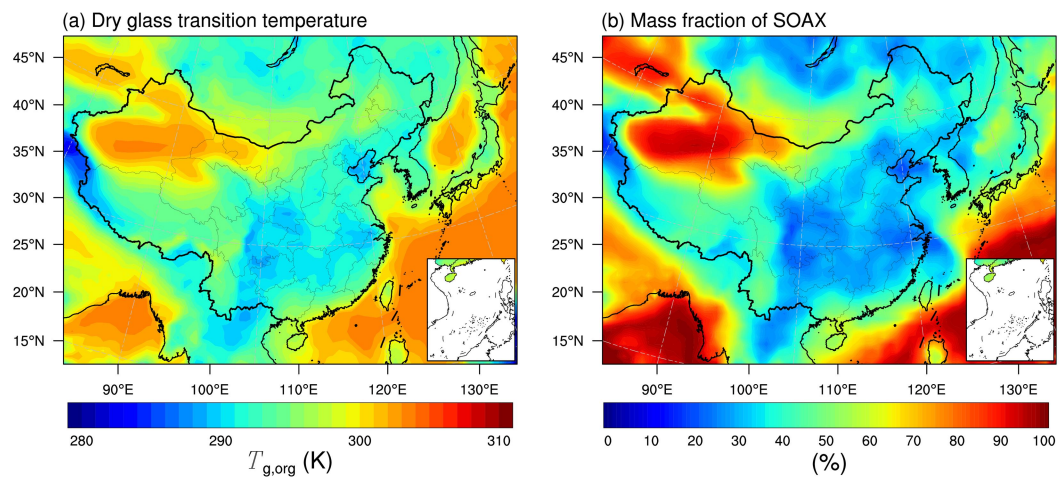
Figure 4. The predicted median surface values of (a) glass transition temperature of SOA particles at the dry condition and (b) mass fractions of SOAX ($C^* = 0.1$ μg m^{-3} at 298 K) during May 20 – June 23 in 2018 simulated in the base case (Table 1).
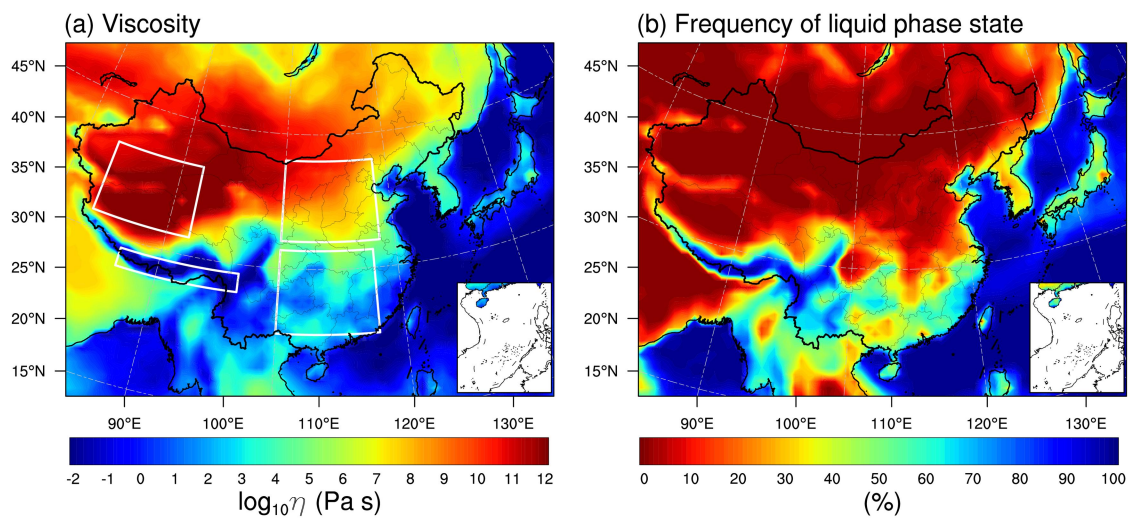
Figure 5. WRF-Chem predicted (a) median surface values of viscosity and (b) the percent time that an organic aerosol particle is in the liquid phase state during May 20 – June 23 in 2018. The white boxes in panel (a) specify the selected regions in the northern China, southern China, northern Qinghai-Tibet Plateau, and southern Qinghai-Tibet Plateau.
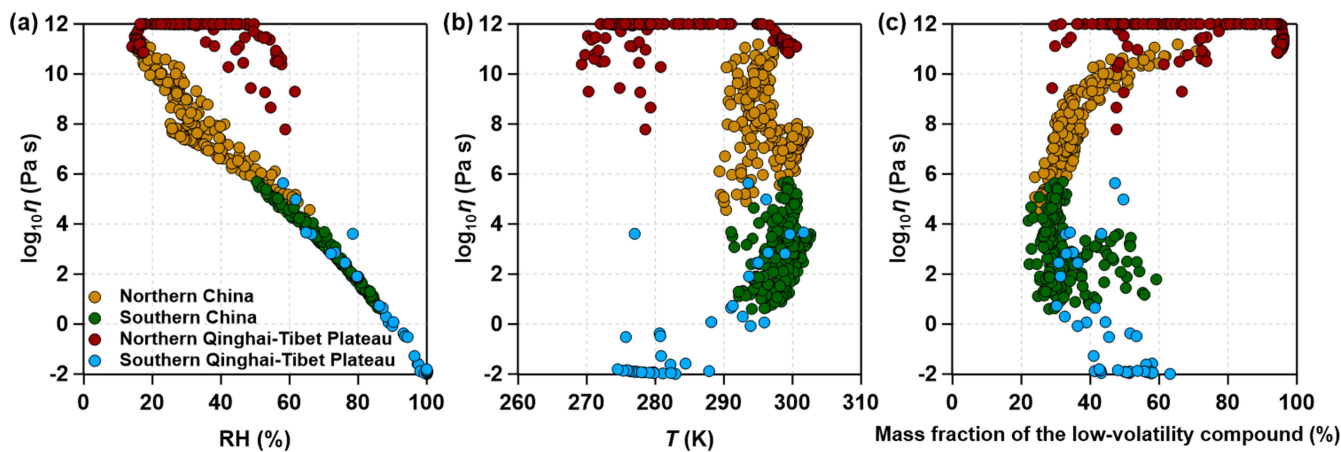
Figure 6. The median values of viscosity as a function of (a) RH, (b) T and (c) the mass fraction of SOAX ($C^* = 0.1$ μg m^{-3} at 298 K) calculated for selected regions in the northern China, southern China, northern Qinghai-Tibet Plateau, and southern Qinghai-Tibet Plateau as specified by white boxes in Fig. 5a during May 20 – June 23 in 2018.
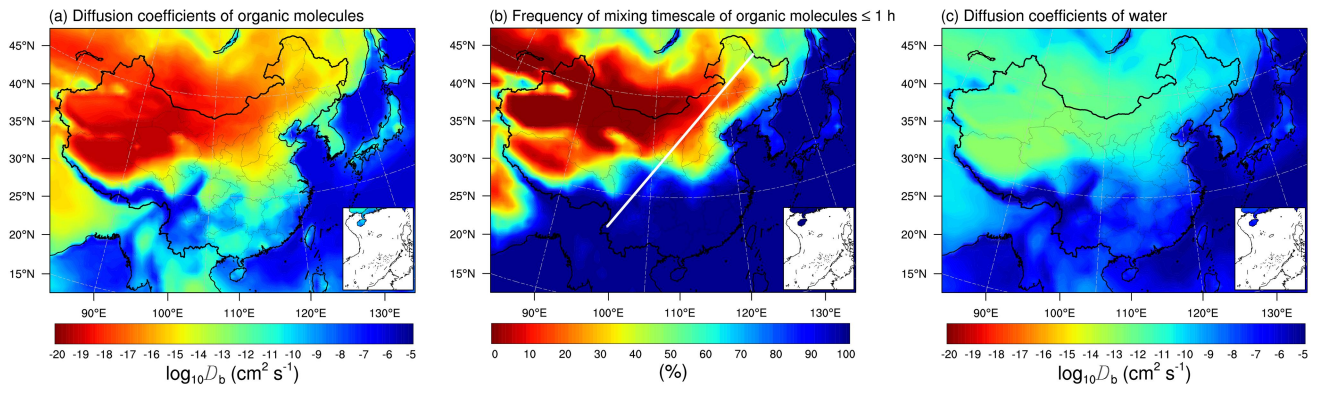
Figure 7. WRF-Chem predicted median surface values of the diffusion coefficients of (a) organic molecules and (c) water molecules in SOA particles. (b) The percent time that the mixing timescale of organic molecules in a 200 nm particle is less than 1 h during May 20 – June 23 in 2018. The white line indicates the "Hu Huanyong Line" (Hu, 1935).
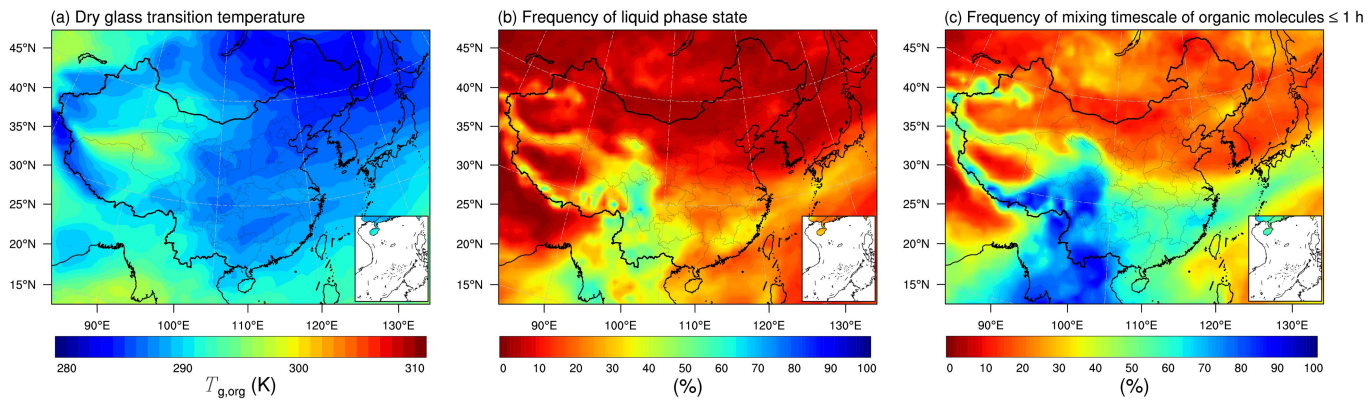
Figure 8. WRF-Chem predicted median values of (a) glass transition temperature of SOA particles at the dry condition, (b) the percent time that an organic aerosol particle is in the liquid phase state, and (c) the percent time that the mixing timescale of organic molecules in a 200 nm particle is less than 1 h at 500 hPa during May 20 – June 23 in 2018.
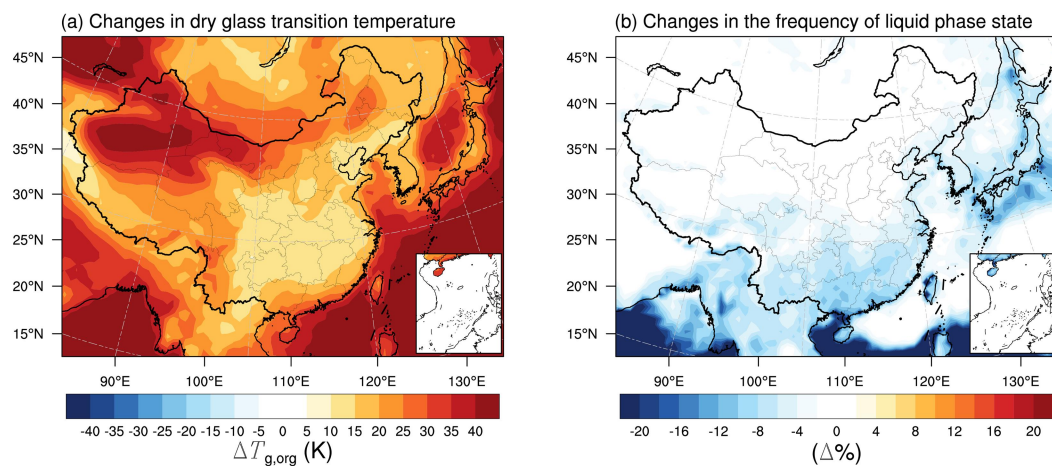
947

948 **Figure 9.** Modelled median differences of (a) glass transition temperature of SOA particles at the dry condition, and (b) the percent time

949 that an organic aerosol particle is in the liquid phase state between a sensitivity case with the lowest C^* of 0.0001 μg m^{-3} at 298 K (ΔH_{vap} of

950 40 kJ mol^{-1}, case A in Table 1) and a base case with the lowest C^* of 0.1 μg m^{-3} at 298 K (ΔH_{vap} of 142 kJ mol^{-1}, Table 1).

951

952

953

954

955

956

957

958

959

960
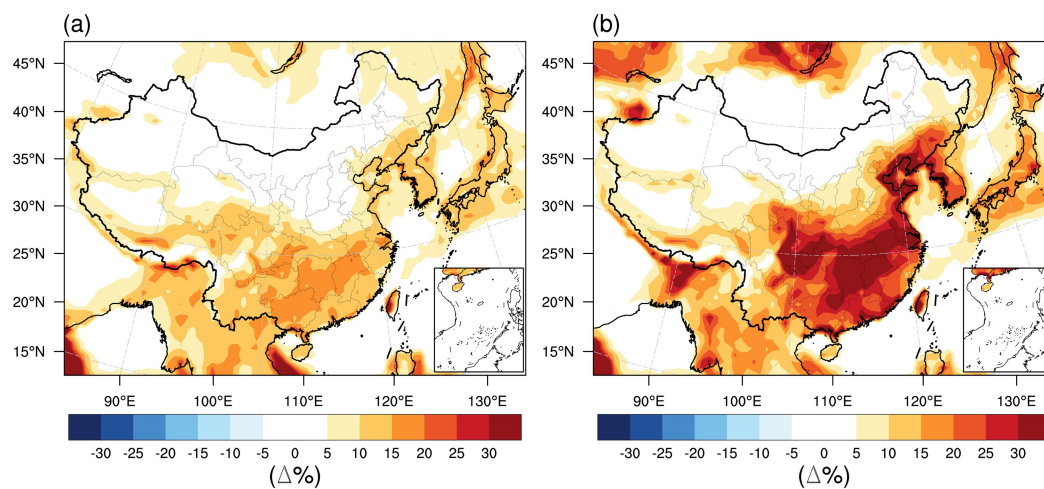
961
962 **Figure 10.** (a) Impacts of RH on the percent time that an organic aerosol particle is in the liquid phase state: modelled median differences
963 between a case with the WRF-Chem simulated RH increased by a factor of 10 % (case B, Table 1) and a base case (Table 1) with the
964 WRF-Chem simulated RH. (b) Impacts of the water absorbed by inorganics on the percent time that an organic aerosol particle is in the
965 liquid phase state: modelled median differences between a case considering the water absorbed by both SOA particles and inorganics (case
966 C, Table 1) and a base case (Table 1) considering the water absorbed by SOA particles solely.

967
968